UNIVERSITY OF TWENTE

MASTER THESIS

Partial volume and T_1 correction in brain magnetic resonance spectroscopy imaging

Improving data processing in order to determine brain glutamate levels in patients who experienced a psychosis

---

Author:
Lisan MORSINKHOF, BSc

Supervisors:

Dr. C.H. RÖDER	Medical supervisor
Dr. A. BHOGAL	Technical supervisor UMCU
Dr. ir. J. WIJNEN	Technical supervisor UMCU
Dr. ir. F.F.J. SIMONIS	Technical supervisor UT
Drs. A.G. LOVINK	Professional behaviour supervisor
Prof. dr. ir. C.H. SLUMP	Chairman and external member

September 2, 2019

UNIVERSITY OF TWENTE.

UMC Utrecht

UNIVERSITY OF TWENTE

Abstract

University Medical Center Utrecht - Imaging division

Partial volume and T_1 correction in brain magnetic resonance spectroscopy imaging

Improving data processing in order to determine brain glutamate levels in patients who experienced a psychosis

by Lisan MORSINKHOF, BSc

Purpose: To correct glutamate concentrations measured using magnetic resonance spectroscopy imaging at 7 Tesla for partial volume and T_1 effects in order to perform a more accurate evaluation of brain glutamate levels in patients who experienced a psychosis.

Methods: Glutamate was denoted as the sum of glutamate and glutamine (Glx) with the total amount of creatine (tCr) as scaling factor. Anatomical data were used to obtain probability fraction maps. These maps were corrected for the voxel bleeding effect in order to relate them to the Glx/tCr maps. Based on these fraction maps and subject specific grey and white matter Glx/tCr concentrations partial volume correction was performed. Subsequently the maps were corrected for the effect of T_1 relaxation. The Wilcoxon signed rank test was used to evaluate the effect of the corrections in several brain regions.

Results: Statistically significant differences in Glx/tCr concentrations were detected in each of the regions. Partial volume correction resulted in an increase of the Glx/tCr concentration in in cortical grey matter, caudate, putamen en thalamus, and a decrease in white matter and the pallidum.

Conclusion: After partial volume and T_1 correction the Glx/tCr concentrations calculated per region were in line with previous studies. Although the actual concentrations were not known, based on comparison of the calculated Glx/tCr concentrations with literature it can be suggested that the corrected concentrations are more accurate than the uncorrected. It has to be evaluated if partial volume and T_1 correction result in a more accurate comparison Glx/tCr concentrations between patients who experienced a psychosis and healthy control subjects.

Keywords: Magnetic resonance spectroscopy imaging, glutamate, partial volume effect, T_1 relaxation

Abbreviations

B_0	static magnetic field
B_1	readiofrequency field
CSF	cerebrospinal fluid
FA	flip angle
FOV	field of view
FWHM	full width half maximum
Gln	glutamine
Glu	glutamate
Glx	glutamate + glutamine
GM	grey matter
MNI	Montreal Neurological Institute - brain standard space
MRS	magnetic resonance spectroscopy
MRSI	magnetic resonance spectroscopy imaging
NMDA	N-methyl-D-aspartate
PSF	point spread function
ROI	region of interest
SNR	signal to noise ratio
SVS	single voxel spectroscopy
tCr	total creatine; creatine + phosphocreatine
TE	echo time
TR	repetition time
WM	white matter

Contents

Chapter 1

Introduction

Psychosis and schizophrenia are among the most burdensome disorders worldwide [1]. Not only do these disorders have a large impact on the patients themselves, it also impacts family members and the community, and has large economic cost. The current pharmacological treatment of psychotic disorders is unable to address all symptoms [2]. To enable a specific treatment, more insight in the neurobiology underlying psychotic disorders is needed [3]. Previous research suggests that glutamate may be a relevant factor in the neurobiology of psychosis, based on findings using magnetic resonance spectroscopy (MRS) [4]–[13]. Nonetheless, for a more accurate determination of glutamate levels, data processing has to be improved. This study seeks to improve the processing method of MRS data. This chapter describes the needs for research into the neurobiology underlying psychotic disorders and improvement of MRS data processing.

1.1 Psychosis and schizophrenia

1.1.1 Definitions

Psychosis is defined as the presence of delusions and/or hallucinations [14]. Delusions are described as fixed false beliefs. Hallucinations are perceptions without the presence of an external or somatic stimulus [14]. Delusions and hallucinations are also called positive symptoms [15], since they indicate the presence of aberrant functioning [16].

The most severe disorder in which psychosis occurs is schizophrenia [1], [17]. In addition to these aforementioned positive symptoms also cognitive impairment and negative symptoms, which are described as a significant deficiency in normal functioning, are present. Negative symptoms such as lack of motivation and social withdrawal are present in this disorder [15].

1.1.2 Current treatment

At the moment the diagnosis of psychotic disorders is mainly based on descriptive psychopathology instead of etiology and biological findings [18]. The link between the psychopathology and the pathophysiology of psychosis is still unclear; however, several theories exist. One theory indicates psychosis as a disorder of aberrant salience [19], [20]. This theory suggests that there is a dysregulation in dopamine transmission. Under normal circumstances dopamine functions as a mediator of relevant saliences. However, due to dysregulation of dopamine transmission, stimuli in the dopaminergic system that are normally insignificant become relevant. The current treatment of schizophrenia, which is based on antipsychotic drugs that block dopamine D2 receptors [21], is in line with the aberrant salience theory.

Nonetheless, inconsistencies concerning the treatment remain. Firstly, clear evidence for the theory of aberrant salience is lacking [18]. Several studies have shown an increase in dopamine synthesis and release in the acute state of schizophrenia [22], [23]. However, this does not prove the causality between dopamine dysfunction and aberrant salience. Secondly, there is a large variation in outcomes after a first episode of psychosis when dopamine based drugs are used. Functional adjustment in the psychological, social and occupational field (e.g. making friends and/or affective relationships outside the family) two years after a first episode of psychosis varies from functional deterioration to an even increased level of functioning [24]. Thirdly, dopamine antagonists hardly affect cognitive and negative symptoms of psychotic disorders [2], [25]. Thus, to obtain specific treatment strategies, understanding of neurobiology underlying psychotic disorders is required [3].

1.1.3 NMDA-glutamate hypothesis

In addition to the dopaminergic hypothesis, there is increasing evidence for dysfunction of the glutamate-gated N-methyl-D-aspartate (NMDA) receptor during psychosis and schizophrenia [26]. The receptor is an ion channel that plays an important role in the excitatory synaptic transmission of the central nervous system [27]. There are several findings that support the NMDA-glutamate hypothesis. Antagonists of this receptor such as phencyclidine and ketamine induce psychotic reactions in patients [28], including negative symptoms and cognitive impairments that do not arise when dopaminergic antagonists are applied [2]. Furthermore, glutamate levels increase in medication-naïve or medication free schizophrenia patients [11]. It is also known that the glutamate level decreases progressively with age in schizophrenia patients compared to healthy controls [13]. These findings suggest that NMDA-receptors are involved in psychotic disorders, warranting further investigation in their role in the neurobiology underlying psychosis.

1.2 Magnetic resonance spectroscopy

Measuring NMDA-receptor function in vivo is challenging. However, since we know that glutamate is its antagonist and therefore intimately involved with this receptor, methods to measure glutamate provide a potential alternative. Using ^{1}H MRS it is possible to measure glutamate concentrations in the brain [13]. In the past several years many papers about ^{1}H MRS of brain glutamate in schizophrenia using 1.5-4T MRI have been published [11]–[13]. The drawback of these studies is the low field strength. Since magnitude of the net magnetization is directly related to the magnetic field strength [29], the signal to noise ratio (SNR) is lower at lower field strengths. This limits the spatial resolution [30]. Furthermore, at lower field strength the dispersion of resonance frequencies between metabolite peaks are small, which makes it difficult to distinguish the different peaks in a metabolite spectrum. Due to these factors it is challenging to draw proper conclusions about the distribution of glutamate levels.

At higher magnetic field strength spatial dispersion will increase, enabling a more accurate calculation of glutamate levels in the brain. Furthermore, the SNR increases, which enables scanning at higher resolution or faster scanning. In single voxel spectroscopy (SVS) this SNR is even higher because many signal averages can be obtained [31]. This is possible due to the fast acquisition time because of a small

region of interest (ROI) [32]. Therefore, this technique is used widespread to measure glutamate concentrations in people with psychotic disorders [4]–[9]. However, the main drawback of these studies is that due to SVS the glutamate concentrations are only measured in a small number of regions, which is inconsistent with the theory that glutamate levels are probably not equally distributed across different brain regions [33]. Using magnetic resonance spectroscopy imaging (MRSI) instead of SVS enables measuring a whole brain slice instead of only a large voxel.

In this study we aim to measure glutamate levels in the brain using MRSI at a magnetic field strength of 7T. An overview of the MRS technique is described in Appendix A. Along with the possibilities of MRSI at 7T also some challenges arise, which are described below.

1.2.1 Partial volume effect

Even at a magnetic field strength of 7T, the SNR of the MRSI data is low due to the low concentration of metabolites. By way of comparison, the number of protons of metabolites, which is related to the area of the peak in a spectrum, is several thousand times lower than that of water [31]. Therefore, the data will be obtained at a resolution of $5\times5\times10\text{mm}^3$, in contrast with the anatomical T_1 data, which can be acquired at a resolution of $1\times1\times1\text{mm}^3$. Because of the low resolution of the MRSI data, there will be a partial volume effect, which means that voxels consist of fractions of different tissue types (grey matter (GM), white matter (WM) and cerebrospinal fluid (CSF)). Each of these tissue types contain a different concentration of glutamate [34]. However, due to the low resolution of the MRSI data, the concentrations within an MRSI voxel will be averaged. To correct for the dependence of the glutamate concentration on the tissue type it is required to correct for this partial volume, which can be performed using information of the anatomical T_1 data with a higher spatial resolution.

1.2.2 Voxel bleeding effect

The obtained signal in a specific MR(S)I voxel is not only originating from the desired voxel, but also from adjacent voxels [35]. This occurs because more frequencies are used to obtain the signal due to finite scan time. As a result, the shape of the signal is not the desired rectangle, indicated by the black line in Figure 1.1, but a sinc function, indicated by the green line. This effect, called voxel bleeding, increases with a decreasing spatial resolution [36]. This means that the voxel bleeding effect is higher in the MRSI data than in the anatomical data.

Because a high lipid signal is obtained from the skin and skull, there is a large voxel bleeding effect of this signal on the MRSI data [36]. This leads to a distortion of the MRS signal of brain metabolites. Therefore, a crusher coil is used to distort the lipid signal during the acquisition of the MRSI data [37].

Although the influence of the voxel bleeding effect of brain tissue is smaller than of the skin and skull, because the lipid signal in the brain tissue is much smaller, the effect still exists in the obtained MRSI signal. This means that voxels do not contain the same tissue composition as the high resolution anatomical data measured at the same location, but is also influenced by signal of surrounding voxels. To achieve an accurate partial volume correction, the anatomical data has to be corrected for this effect before they can be related to the MRSI data [38].

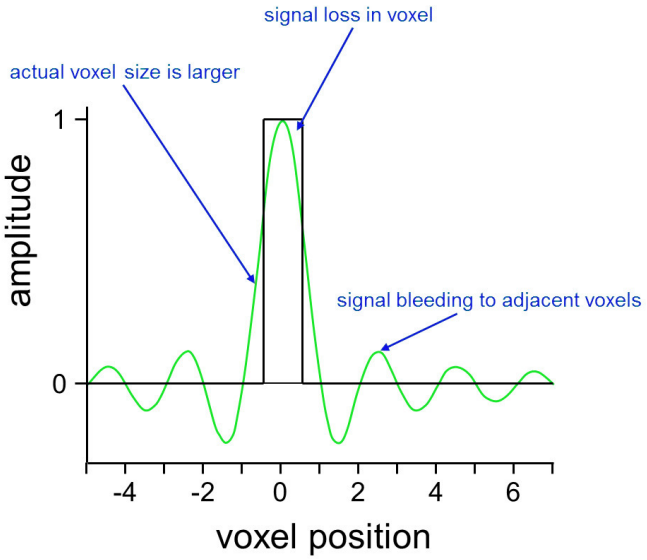

FIGURE 1.1: The consequences of finite scan time. The black line indicates the desired signal shape: equal to the voxel size. The green line indicates the real signal shape: a sinc function. This has three consequences: 1) in the actual voxel there is a signal loss, 2) bleeding of the signal into other voxels occurs, 3) the actual voxel size is larger than the original voxel. Adjusted from de Graaf et al. [35].

1.2.3 T_1 effect

To reduce the acquisition times using MRSI, a short repetition time (TR) is used during acquisition. This is performed using a low excitation flip angle (FA) in order to receive data with a SNR as high as possible. When this TR is shorter than the longitudinal relaxation time (T_1), the magnetization cannot totally recover, resulting in a reduction of the signal [39]. Therefore, the area underneath a metabolite peak, is not directly related to the metabolite concentration anymore, but is underestimated [39], [40]. However, to acquire a fully relaxed spectrum, the repetition time (TR) has to be at least five times longer than T_1 [39]. This results in a TR of 8.75 seconds for glutamate [40], leading to very long acquisition times. To decrease the acquisition times, a shorter TR can be used, but to prevent underestimation of the metabolite concentrations, correction for the T_1 effect has to be performed [40], [41].

The T_1 relaxation times of metabolites are different in GM and WM. For glutamate these times are 1.61 and 1.75 seconds respectively [40]. Partial volume correction enables correction for the T_1 effect based on the T_1 relaxation times per tissue type.

1.3 Aim and hypothesis

The main goal of this study is to correct for the partial volume and T_1 effects of the MRSI data in order to achieve a more accurate representation of glutamate levels in the brain. This based on the fact that tissue specific glutamate concentrations are taken into account and the metabolite signals are not underestimated anymore. We hypothesize that due to partial volume correction the glutamate concentration increases in GM and decreases in WM and CSF. Furthermore, it is hypothesized that T_1 correction increases metabolite concentrations.

Due to the corrections the quality and reliability of the high resolution MRSI data will be improved. This enables a more accurate determination of glutamate levels in the brain and comparison of the levels between patients who experienced a psychosis and healthy control subjects. In this way more insight into the neurobiology of psychotic disorders can be gained, which may result in better treatments.

Chapter 2

Methods

2.1 Subject inclusion

2.1.1 Subjects

This study was approved by the medical research ethics committee of the University Medical Center Utrecht (protocol ID NL55796.041.15). All subjects provided written informed consent. The subjects were enrolled from advertisements on posters and an independent website for test subjects for clinical trials. In total 29 healthy control subjects (20 males) with a mean (SD) age of 24.5 (7.5) years were included between October 2017 and July 2019. Two subjects were not scanned because of claustrophobia. Four data sets were incomplete due to saving and processing problems. Therefore, the number of data sets used for analysis was 23.

2.1.2 Data acquisition

The data was acquired using an existing scan protocol. A 7 Tesla Achieva Magnetic Resonance System (Philips, Best, NL) with a 32 channel receive head coil (Nova Medical, Wilmington MA, USA) is used for acquisition. An overview of the parameters of the different scans is shown in Table 2.1.

Anatomical data

A map of the static magnetic field (B_0) was achieved to detect inhomogeneities. This map was used to calculate the shim values applied during acquisition of the MRSI data in order to improve the B_0 field homogeneity. For anatomical reference a 3D magnetization prepared rapid gradient-echo (MPRAGE) image was acquired. A 2D multislice T_1-weighted fast field echo (2D FFE) image was obtained to test the crusher coil. Based on the 3D MPRAGE image a reconstruction of these 2D anatomical scans, consisting of 20 slices with a thickness of 1mm, was created on the scanner. This is followed by a shimmed B_0-map and a map of the radiofrequency field (B_1) to map the B_1 and remaining B_0 inhomogeneities. These maps are used for line width correction in the post-processing phase.

MRSI data

The ^{1}H-MRSI data was acquired in two slices containing subcortical GM nuclei. Lipid signals were suppressed using a crusher coil [37]. Homogeneous water suppression was obtained using tailored spiral in-out spectral-spatial radiofrequency (RF) pulses based on the B_0 and B_1 maps [42], by the RF chemical shift selective (RF CHESS) method. Shimming was applied based on the calculated shim values from the B_0-map. In the same region non-water suppressed data was acquired.

TABLE 2.1: Parameters used per scan. TE: echo time, TR: repetition time, FOV: field of view, FA: flip angle, NSA: number of signal averages

	B_0 and B_1	MPRAGE	2D FFE	MRSI WS*	MRSI non-WS*
TE (ms)	2.35	2.89	4.22	2.5	2.5
TR (ms)	5.122	8	200	300	300
FOV (mm^3)	220×220×30	220×220×200	220×220×20	220×220×10	220×220×10
Resolution (mm^3)	1.25×1.25×10	1×1×1	1.25×1.25×10	5×5×10	10×10×10
FA (degrees)	-	6	-	35	35
Number of slices	3	-	2	2	2
NSA	-	-	-	2	2
Scan time (min)	1:06	6:51	1:12	10:59	1:54

*In one subject only one slice was acquired. In two subjects three slices with a resolution of 5×5×5 mm^3 instead of two slices with a resolution of 5×5×10mm^3 were obtained

2.2 Data processing

The acquired ^{1}H-MRSI data were processed using an existing pipeline. The first step in this pipeline is reconstruction and post-processing of the data using FidGet, a program for optimization of the ^{1}H-MRSI data developed at the Max Planck Institute for Biological Cybernetics (Tuebingen, Germany) [43]. The reconstruction steps of FidGet contain of k-space filtering with a squared Hamming window, in order to reduce the voxel bleeding effect [36], and overdiscrete B_0-correction, resulting in a higher signal to noise ratio (SNR) and smaller full width half maximum (FWHM) [44]. During post-processing missing point prediction [43], [45], eddy current correction, zero order phase correction [46] and removal of the residual water peak [45] are performed.

After reconstruction and post-processing metabolite quantification was performed using the linear combination fitting program LCModel (version 6.3-1K) [47]. The metabolites are quantified by fitting of a series of basis functions of metabolite spectra to the acquired data (see Figure 2.1) using the control parameters shown in Appendix B. The absolute metabolite concentrations as well as the concentrations with the total amount of creatine (tCr = creatine + phosphocreatine) as scaling factor were calculated. In this study the concentrations with tCr as scaling factor were used for further calculations. This is done to overcome the problem of the variability in flip angle across the brain due to B_1 inhomogeneity, which influences the calculated metabolite concentrations [48]. tCr is often used as reference since it is assumed to be among the three metabolites (next to N-acetylaspartate and choline) of which the concentrations are stable within most of the brain conditions [30].

Together with the metabolite concentrations quality assurance data, consisting of the standard deviation compared with the Cramér-Rao lower bounds (CRLB, certainty of metabolite concentration), the FWHM and SNR of the fitted spectra, were calculated by LCModel. These data were used to perform quality control, using Matlab R2017b (MathWorks, Natick MA). Voxels with SNR < 3, FWHM > 0.15 ppm, CRLB < 50% or a lipid over creatine ratio higher than 2 were excluded to obtain reliable metabolite maps. Remaining voxels with a metabolite over tCr ratio higher than 5 that were not excluded during quality control were removed afterwards.

After quality control the metabolite maps were transformed to the Montreal Neurological Institute (MNI) 152 standard brain (6^{th} generation). The transformation is

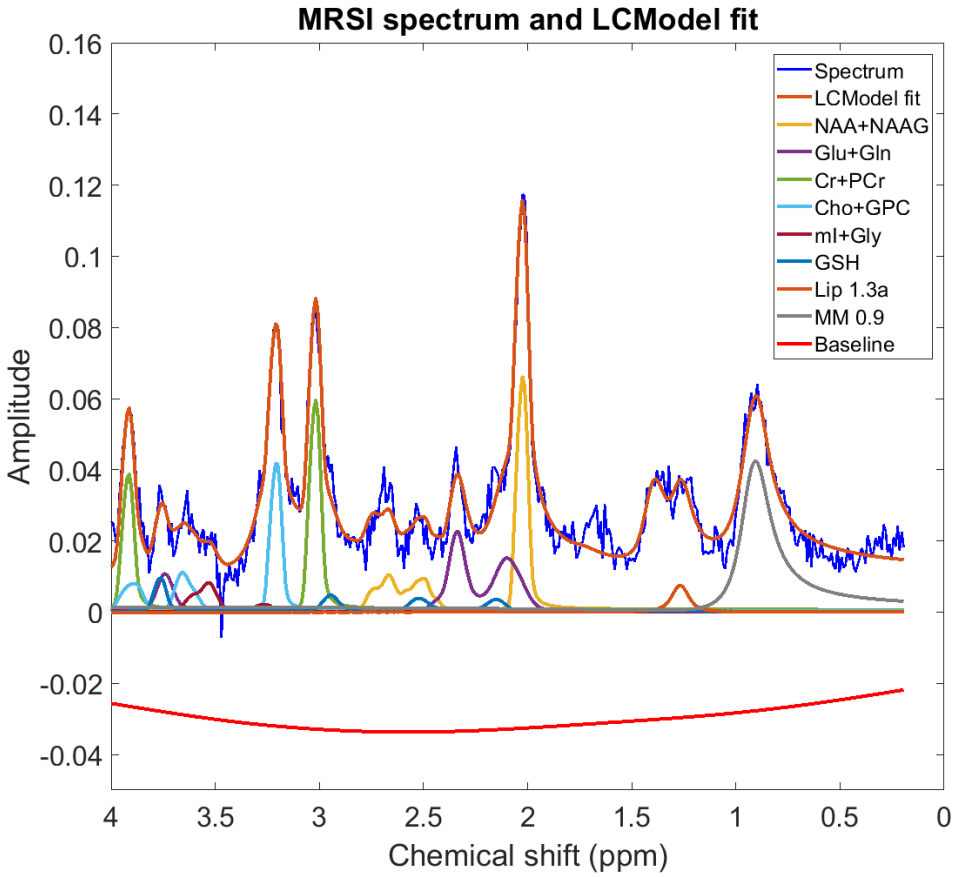

FIGURE 2.1: MRSI spectrum including the fitted metabolites and the total fit of LCModel (LCModel fit). NAA: N-acetylaspartate, NAAG: N-Acetylaspartylglutamate, Glu: glutamate, Gln: glutamine, Cr: creatine, PCr: phosphocreatine, Cho: choline, GPC glycerophosphocholine, mI: myo-inositol, Gly: glycine, GSH: glutathione, Lip13a: lipid at 1.3ppm, MM 0.9: macromolecule at 0.9ppm

performed using FSL (FMRIB Software Library, Oxford, UK). First, the anatomical 2D slices are linearly registered to the T_1 weighted 3D volume (slice-to-3D). Thereafter, the T_1 weighted 3D volume was transformed from subject to MNI space by linear and non-linear transformation [49], [50]. The transformation matrix corresponding to the transformation of the T_1 weighted 3D volume to MNI space was used to transform the anatomical slice to MNI space. MRSI data were transformed to MNI space using the transformation matrices corresponding to the slice-to-3D and 3D-to-MNI transformations.

2.3 Corrections

The corrections were performed using Matlab R2017b (MathWorks, Natick MA). They were implemented in the pipeline before transformation of the metabolite maps to MNI space.

2.3.1 Partial volume calculation

Partial volume correction was performed by a redistribution of the metabolite signal within a voxel. This redistribution is based on the fraction of GM, WM and CSF in the corresponding voxels of an anatomical T_1-weighted scan with a higher resolution. Calculation of the fraction maps in order to correct for the partial volume effect was performed by segmentation of an anatomical reference scan with a resolution of 1x1x1 mm^3 into the tissue types GM, WM and CSF. This was achieved using the FMRIB's Automated Segmentation Tool (FAST) of FSL [51].

First, the segmentation was performed in subject space. However, due to inhomogeneities in the intensity of the anatomical data, these segmentations were not successful in all subjects. An example of one of these subjects is shown in Figure 2.2. Therefore, it was decided to perform the segmentation in MNI space and transform the obtained tissue maps back into subject space.

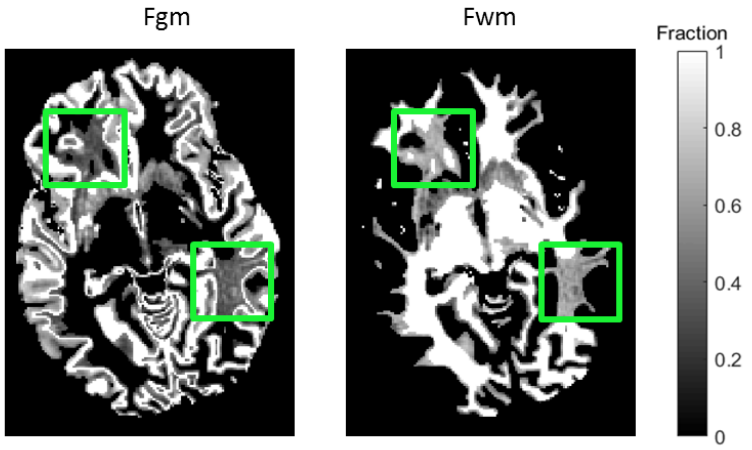

FIGURE 2.2: Example of GM and WM segmentations in subject space. The green boxes indicate regions in which WM is partly segmented as GM. Because of the incorrect segmentations in some subjects it was decided to perform segmentation in MNI instead of subject space.

By using binary tissue maps, some parts of GM nuclei were not recognized and labeled as WM (see Figure 2.3). Because partial volume correction is based on differences in GM and WM, the correction in these regions did not succeed. For that reason it was chosen to use probability tissue maps instead of binary maps. Based on visual inspection it was concluded that in these probability maps the labeling of the nuclei was more accurate.

2.3.2 Correction for voxel bleeding effect

To take into account the proper GM, WM and CSF contributions during correction for the partial volume effect, the voxel bleeding effect of the MRSI data has to be applied to the fraction maps. This is performed by a convolution of the maps with a 2D filter. This filter is created in a couple of steps, shown in 1D in Figure 2.4. First, a 220×220 matrix of zeros was generated to resemble the 2D field of view (FOV) of an anatomical slice. Within this matrix 5×5 voxels are set to one, indicating the size of one MRSI voxel. This matrix was fourier transformed to k-space domain. To resemble the k-space size of the MRSI voxels, only the center 44×44 voxels of this matrix were kept. Because the k-space was circular, a mask of this k-space was

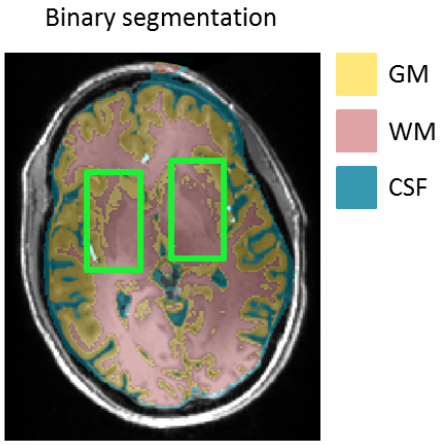

FIGURE 2.3: Example of binary tissue maps of GM, WM and CSF. The green boxes indicate the region containing the putamen (subcortical GM nucleus) that is indicated as WM. Based on these findings it was decided to use probability instead of binary maps.

applied to the center 44×44 voxels of the matrix. The voxels of the 220×220 matrix outside the circular k-space were replaced by zeros. This new matrix was inverse fourier transformed to obtain the filter for application on the fraction maps. Before application the matrix was convolved with a Gaussian to resemble the filtering step of FidGet (section 2.2) in order to reduce the voxel bleeding effect. The obtained filter was scaled in a way that the area under the curve was equal to one. Thereafter, it was convolved with the fraction maps. The fraction maps corrected for the voxel bleeding effect, as shown in Figure 2.5, were used for partial volume correction.

2.3.3 Partial volume correction

The total signal acquired from an MRSI volume (voxel) is the average of all components of that voxel. Because of the large voxel size, different tissue types can be present inside a voxel. Metabolite concentrations differ per tissue type [34]. If there are different tissue types within an MRSI volume, the obtained MRSI signal consists of a mix of signals from these different tissue types. Based on the corrected fraction maps the amount of a certain metabolite inside an MRSI volume can be redistributed inside the same volume. The correction method is explained using an example with one MRSI voxel containing four corresponding anatomical voxels of which the GM, WM and CSF fractions are calculated, as shown in Figure 2.6a and b respectively.

First, the low resolution MRSI voxel was upsampled to a higher resolution. Because the measured concentrations were calculated with tCr as scaling factor, the metabolite concentration of each voxel in a high resolution image has the same concentration as the concentration of the low resolution voxel (see Figure 2.6).

After upsampling the MRSI voxel, the measured concentration was redistributed based on the different tissue types. Factors that influence the measured concentration are the tissue fractions (F) and the tissue specific metabolite concentrations (C) of GM, WM and CSF. Since the metabolite concentration in CSF is in μmol/l order of magnitude [52] and those of GM and WM are in mmol/l respectively [41], [53], [54], it is assumed that the contribution of the metabolite signal of CSF to the total MRSI signal is negligible. Therefore, the tissue fractions have to be corrected for the amount of CSF within a voxel [55]:

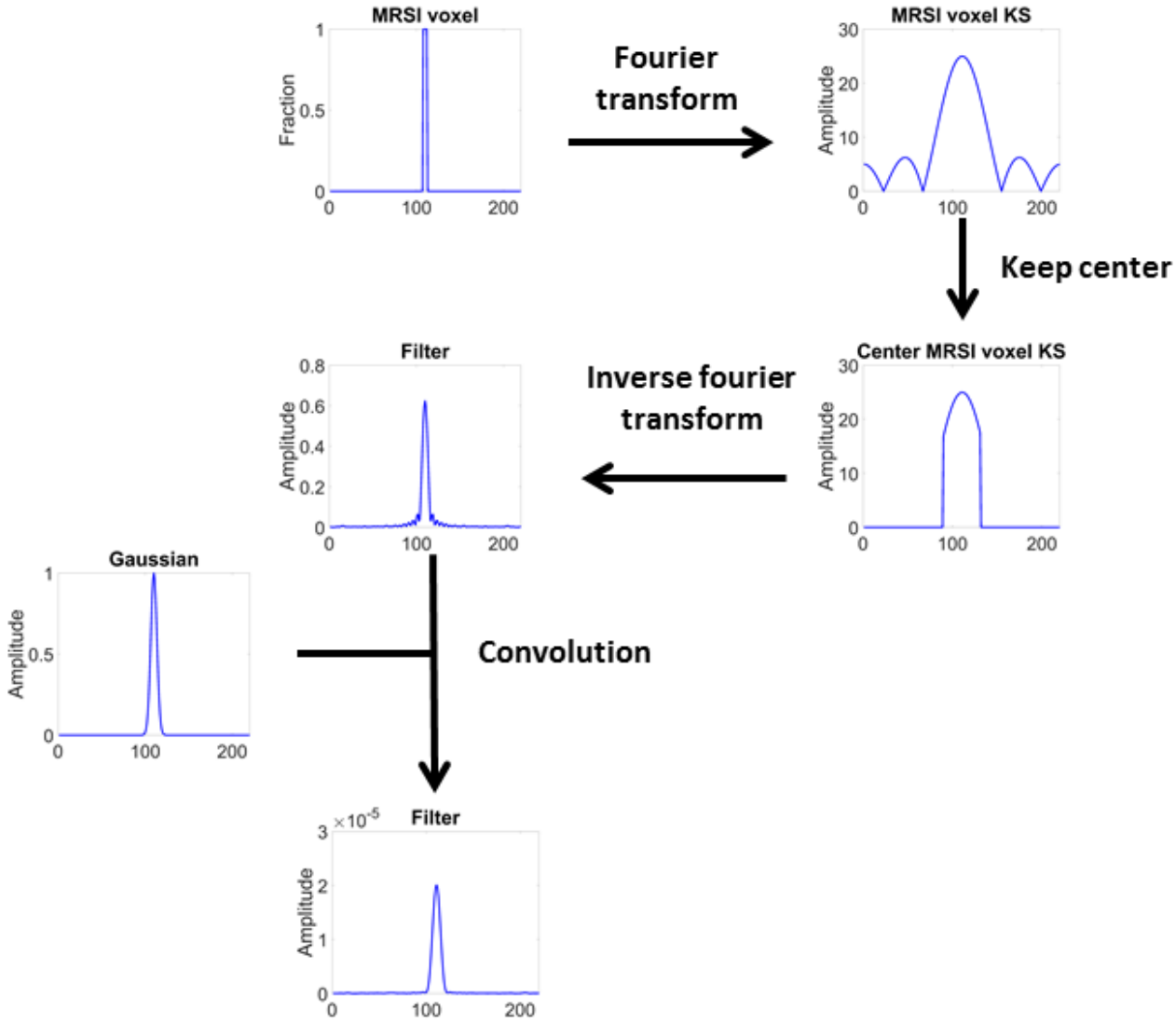

FIGURE 2.4: The filter to resemble the voxel bleeding effect of the MRSI data is created by fourier transformation of a 220×200 matrix, in which 5×5 voxels are set to one to resemble the size of one MRSI voxel. The 44×44 center, representing the size of the MRSI k-space, of this matrix is kept and the rest is replaced by zeros. Inverse fourier transformation of the matrix results in the filter. This filter is convolved a Gaussian to resemble the filtering step of FidGet.

$$X_i = \frac{F_i}{F_{GM} + F_{WM}} \tag{2.1}$$

in which i is the GM or WM tissue. Based on the example in Figure 2.6b these values are 2/3 for X_{GM} and 1/3 for X_{WM} respectively. Using these values the fraction contribution $R_{fraction}$ of the GM and WM tissue to the concentration correction was calculated:

$$R_{fraction} = \frac{X_{GM}}{X_{WM}} \tag{2.2}$$

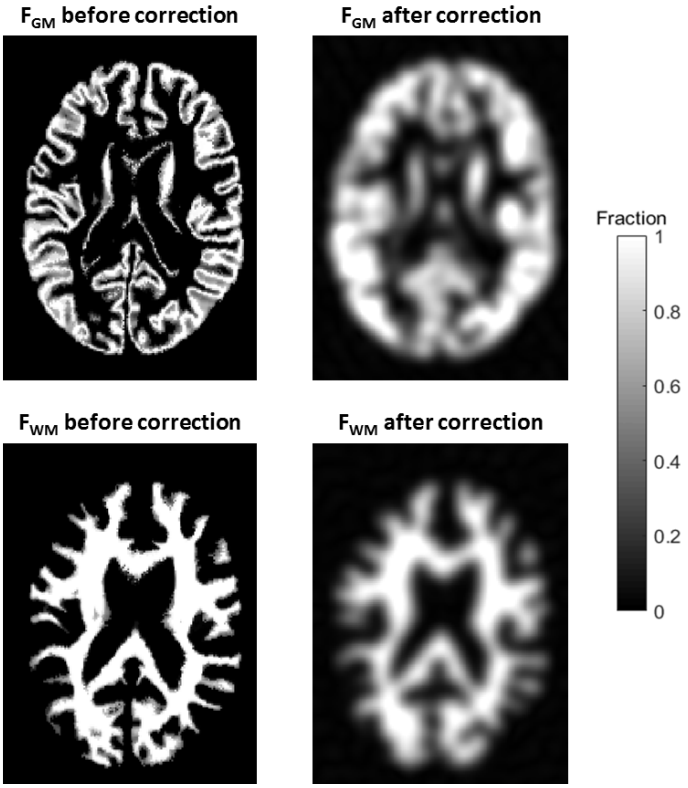

FIGURE 2.5: The effect of correction for the voxel bleeding effect. The left half of the figure shows the GM and WM fraction maps obtained from the anatomical slice respectively. At the right the GM and WM fraction maps after correction for the voxel bleeding effect, which are used for partial volume correction, are presented

In case of the example $R_{fraction}$ is equal to two, which means that the contribution of GM to the measured concentration is two times as high as the contribution of WM.

The contribution of the tissue specific metabolite concentration was determined by plotting the values of X_{GM} of a low resolution anatomical image against the corresponding metabolite concentration. The low resolution anatomical image was created by downsampling the high resolution image to the same resolution as the metabolite image. Using linear regression the values were extrapolated to a concentration of a 100% GM and 100% WM voxel (C_{GM} and C_{WM} respectively), as shown in Figure 2.7 [56]. Subsequently, the concentration contribution to the concentration correction $R_{concentration}$ was calculated using:

$$R_{concentration} = \frac{C_{GM}}{C_{WM}} \tag{2.3}$$

As can be seen from Figure 2.7, in this example C_{GM} is equal to 1.6 and C_{WM} equals 0.8, resulting in a concentration contribution of two. This indicates that the metabolite concentration in GM tissue is two times higher than the concentration in WM tissue. The scatterplot was only created when more than 200 MRSI voxels were available after quality control, in order to obtain reliable values. In other cases $R_{concentration}$ was set to one and the partial volume correction was only based on the fraction contribution.

The total contribution of GM with reference to WM to the signal was calculated using:

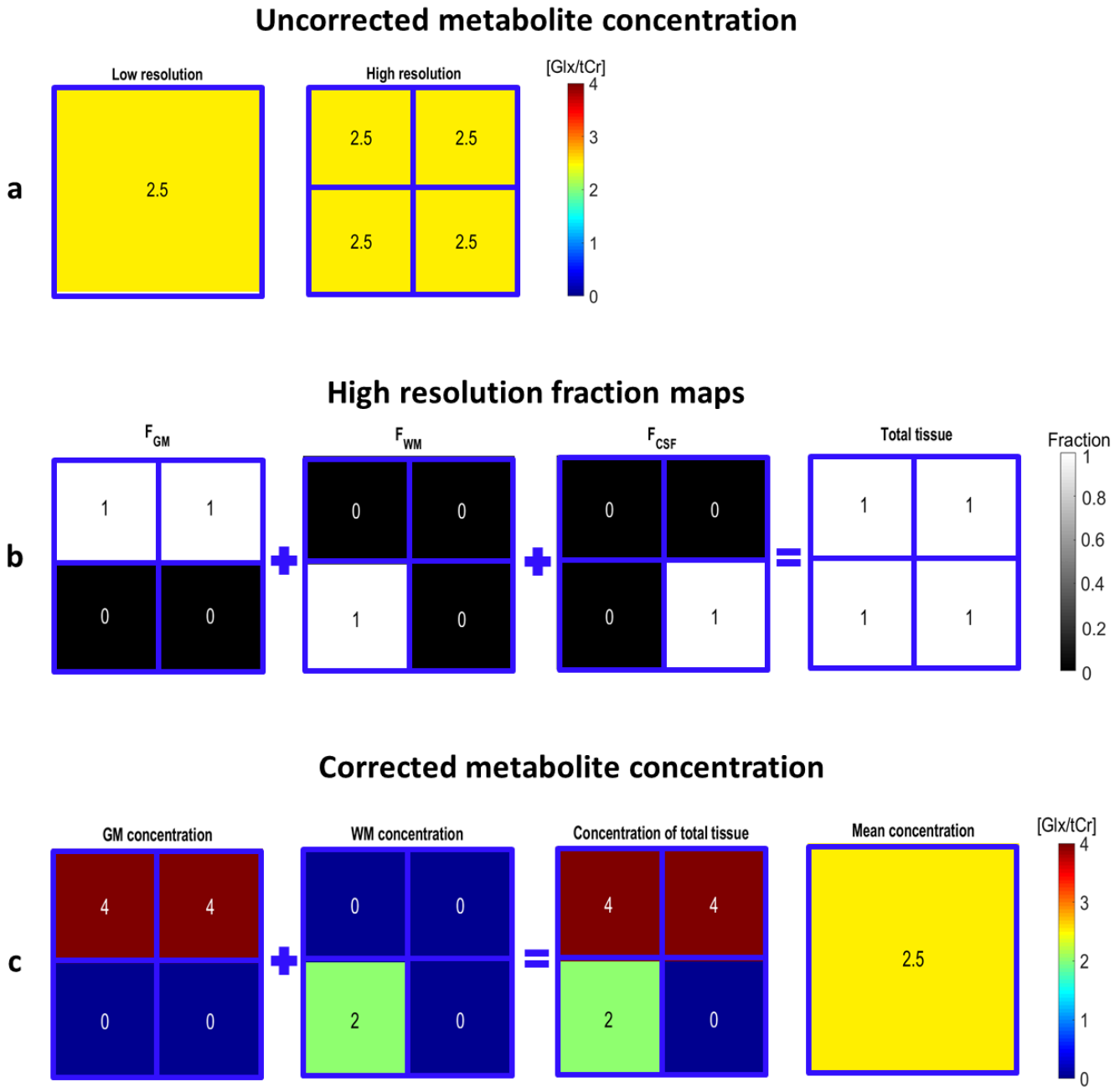

FIGURE 2.6: Example of partial volume correction. The blue boxes indicate the voxel size. The correction is based on a low resolution MRSI voxel that is upscaled to a higher resolution (a) and the corresponding high resolution GM, WM and CSF fraction maps, which together represent the total tissue (b). The corrected concentrations are calculated for GM and WM tissue separately, and can be added up to obtain the corrected concentration of the total tissue (c). The mean concentration of the high resolution corrected voxels is equal to the concentration of the low resolution voxel.

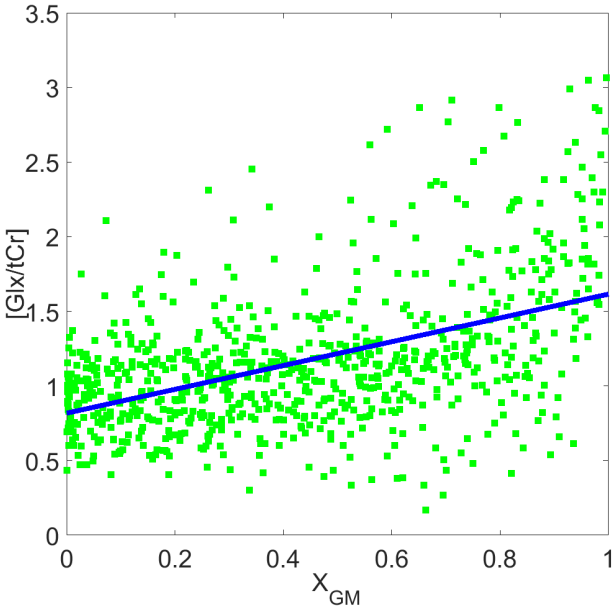

FIGURE 2.7: Scatter plot for determination of C_{GM} ($X_{GM} = 1$) and C_{WM} ($X_{GM} = 0$) using linear regression. Based on this plot the values are 1.6 and 0.8 respectively.

$$R_{total} = R_{fraction} \cdot R_{concentration} \tag{2.4}$$

Thus, based on fraction and concentration, the contribution of GM to the measured metabolite concentration of the example presented in Figure 2.6 is four times as high as the contribution of WM. This indicates that the amount of concentration originating from GM (P_{GM}) is equal to:

$$P_{GM} = \frac{R_{total}}{R_{total} + 1} \tag{2.5}$$

which is 0.8 in this example. The amount of concentration originating from WM (P_{WM}) is

$$P_{WM} = 1 - P_{GM} \tag{2.6}$$

which is 0.2.

The final step was to distribute P_{GM} and P_{WM} over the right voxels based on the fraction distribution. For GM the concentration has to be divided equally to between the upper left and upper right voxel and four WM the total concentration belongs to the lower left voxel, as shown in Figure 2.6c. To obtain the corrected concentration of the total voxel, the GM and WM concentrations are added to each other. The mean of the corrected concentration is equal to the uncorrected metabolite concentration.

2.3.4 T_1 correction

The total measured concentration $C_{measured}$ of a specific metabolite depends on the T_1 and T_2 relaxation times, in the following way:

$$C_{measured} = C_{real,GM} \cdot e^{-\frac{TE}{T_{2,GM}}} \cdot (1 - e^{-\frac{TR}{T_{1,GM}}}) + C_{real,WM} \cdot e^{-\frac{TE}{T_{2,WM}}} \cdot (1 - e^{-\frac{TR}{T_{1,WM}}}) \quad (2.7)$$

In this equation TE is the echo time, TR the repetition time and C_{GM} and C_{WM} the GM and WM concentration respectively. Because the TE used during acquisition of the MRSI data is relatively short (see Table 2.1), $e^{-\frac{TE}{T_2}}$ is assumed to be equal to one. Therefore, equation 2.7 can be reduced to:

$$C_{measured} = C_{real,GM} \cdot (1 - e^{-\frac{TR}{T_{1,GM}}}) + C_{real,WM} \cdot (1 - e^{-\frac{TR}{T_{1,WM}}}) \quad (2.8)$$

Due to the short TR of 300 ms, correction for relaxation parameter T_1 has to be performed to prevent underestimation of the MRSI signal, which is directly related to the metabolite concentration. The real signal can be calculated by:

$$C_{real} = C_{measured} \cdot \frac{1}{1 - e^{-\frac{TR}{T_{1,i}}}} \quad (2.9)$$

in which i is GM or WM. Because our metabolite concentrations weighted over tCr, this also has to be applied to the T_1 correction. This results in:

$$C_{real} = C_{measured} \cdot \frac{1 - e^{-\frac{TR}{T_{1,iref}}}}{1 - e^{-\frac{TR}{T_{1,imtb}}}} \quad (2.10)$$

Using the T_1 relaxation times calculated by Xin et al. [40], as depicted in Appendix C, it can be calculated that $C_{measured}$ for glutamate has to be multiplied with a factor of 0.93 for GM and 0.98 for WM to obtain C_{real} when the scaling factor is tCr.

2.4 Analysis of influence of the corrections on glutamate concentrations

Since the resonance frequencies of glutamate and glutamine are located close to each other, it is difficult to separate the signals of these molecules. To obtain a more robust determination of the glutamate signal, the maps of glutamate and glutamine together (Glx/tCr) are used for analysis.

To analyze the effect of partial volume correction, the mean Glx/tCr concentrations were calculated in the brain regions which are covered by the MRSI slices: WM, cortical GM and subcortical GM nuclei (caudate, pallidum, putamen and thalamus). From these structures the total, center and edge region were analyzed. The regions of these structures were obtained by manually thresholding probability structure maps of the Harvard-Oxford subcortical structural atlas [57] in FSL. To obtain the center parts of the regions the threshold of the probability structure maps was set to a higher level, which differs per region. The resulting center region was approximately 3 voxels (in MNI space) smaller in circumference than the total region. The edge region was defined as the difference between the total and center region masks. An overview of the structures and their total and center regions is depicted in Figure 2.8.

There are two reasons why the edge and center region of the structure were evaluated next to the total structures. First, the effect of the partial volume correction will be less visible in the edge regions, because those regions exist of both GM and WM. Therefore, a decrease as well as an increase in concentration occurs in these

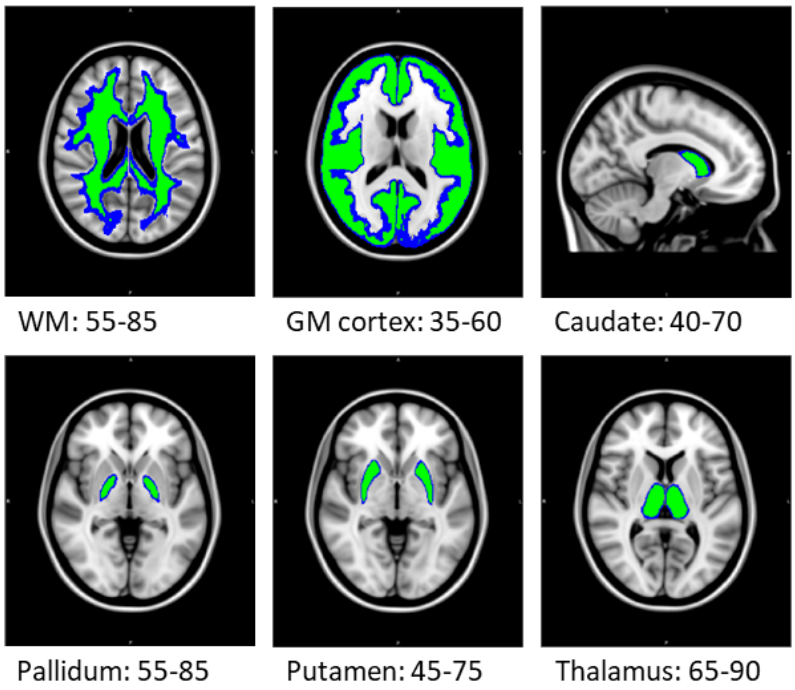

FIGURE 2.8: Brain region masks used for calculation of Glx/tCr concentrations, including the values at which the probability regions are thresholded to obtain the total (blue) and center (green) region respectively.

regions. Second, because the fraction maps are created by segmentation in MNI space and transformation to the 2D slice, there can be a small error in the position of the fraction map compared to the anatomical slice. This error is largest on the edge of the regions due to the difference in GM and WM. Therefore, it is expected that the metabolite concentrations calculated in the center regions of the GM and WM structures are more accurate.

The differences between the total, center and edge regions were analyzed based on the average healthy control maps with and without partial volume correction. Further analysis of the difference between the uncorrected and corrected maps was performed using the individual subject maps. To enable comparison of those maps they were transformed to MNI space. Due to interpolation the resolution of both maps become equal to the resolution of the MNI brain.

The Wilcoxon signed rank test was performed using SPSS 25 (IBM Statistics, Chicago, IL) to analyze if the mean Glx/tCr concentrations in the center parts of the selected structures significantly change after partial volume and T_1 correction. This nonparametric test to compare related samples was chosen because of the small number of healthy control subjects. Because the same test was applied on six different structures, Bonferroni correction was applied by multiplying the resulting p-values by six. Subcortical GM nuclei of subjects in which in less than twenty percent of the total number of voxels the Glx/tCr concentration was calculated were excluded from analysis, because it was assumed that in those cases the number of calculated concentrations is too little to calculate a representative concentration for the total structure. Because the WM and cortical GM structures are larger than the subcortical GM structures, the threshold in those values was set to five percent.

Chapter 3

Results

3.1 Corrections

In one subject the number of voxels left after quality control was less than 200 and therefore partial volume correction was not applied. Therefore, this subject was excluded during analysis.

Figure 3.1 shows the spread of the GM and WM Glx/tCr concentrations between the different subjects, extracted from the scatter plots. It can be noticed that the concentrations were higher in GM than in WM. The WM concentration shows one outlier. However, this subject was not excluded in further analysis because the value is still physiologically realistic.

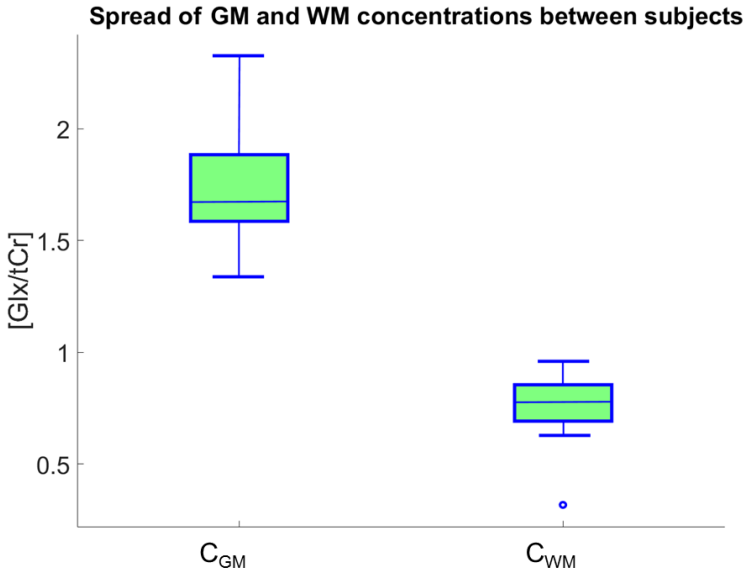

FIGURE 3.1: GM Glx/tCr concentrations are higher than WM.

Figure 3.2 shows the difference in Glx/tCr concentration between the uncorrected and partial volume corrected metabolite maps, ranging between -0.7 and 0.7. It can be noticed from Figure 3.3 that due to partial volume correction the Glx/tCr concentration increased in GM and decreased in WM and CSF. The corrected Glx/tCr concentrations align with the fraction maps corrected for the voxel bleeding effect. According to the histograms shown in Figure 3.4, it can be noticed that the standard deviations of the Glx/tCr concentrations of all regions increased after partial volume correction. Furthermore, it can be seen that partial volume correction resulted in a decrease of the mean Glx/tCr concentration in the WM and

the pallidum. Cortical GM, caudate, putamen and thalamus show an increase in Glx/tCr concentration. These effects mainly occur in the center part of the regions. It can be noticed from Table 3.1 that the decreases of the WM and pallidum were significant, with P<0.001 and P<0.05 respectively. The caudate, putamen, thalamus and cortical GM show a significant increase in Glx/tCr concentration, with P<0.001 for the first three regions and P<0.01 for the last mentioned.

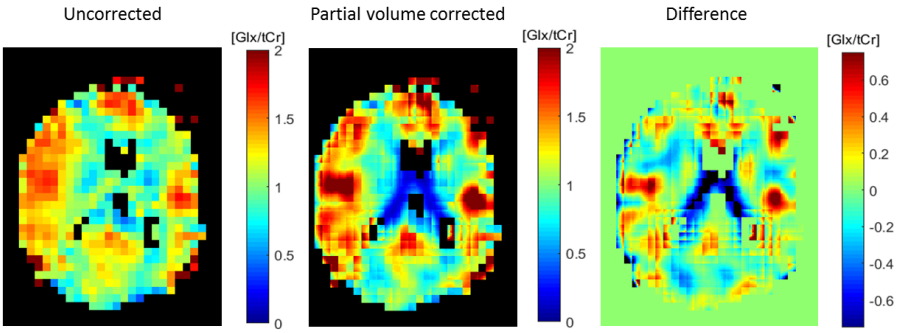

FIGURE 3.2: The effect of partial volume correction. Comparing these figures to the PSF corrected fraction maps of Figure 2.5 can be noticed from the difference map that the [Glx/tCr] concentration increases in GM regions and decreases in WM and CSF regions (according to Figure 2.5).

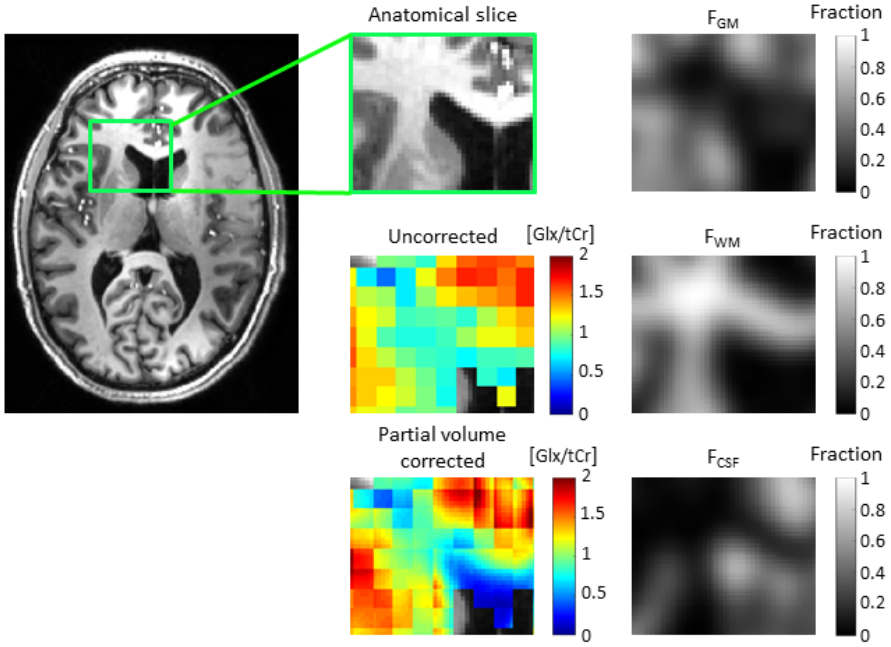

FIGURE 3.3: Comparing the partial volume corrected Glx/tCr map to the fraction maps corrected for the voxel bleeding effect, it can be seen that the concentrations align with the fraction maps. The concentrations increase in GM and decrease in WM and CSF.

T_1 correction resulted in a decrease in Glx/tCr concentrations compared to the partial volume corrected maps (see Figure 3.5 and Table 3.1). This decrease was significant in all regions, with P<0.001 in WM and the thalamus, P<0.01 in cortical

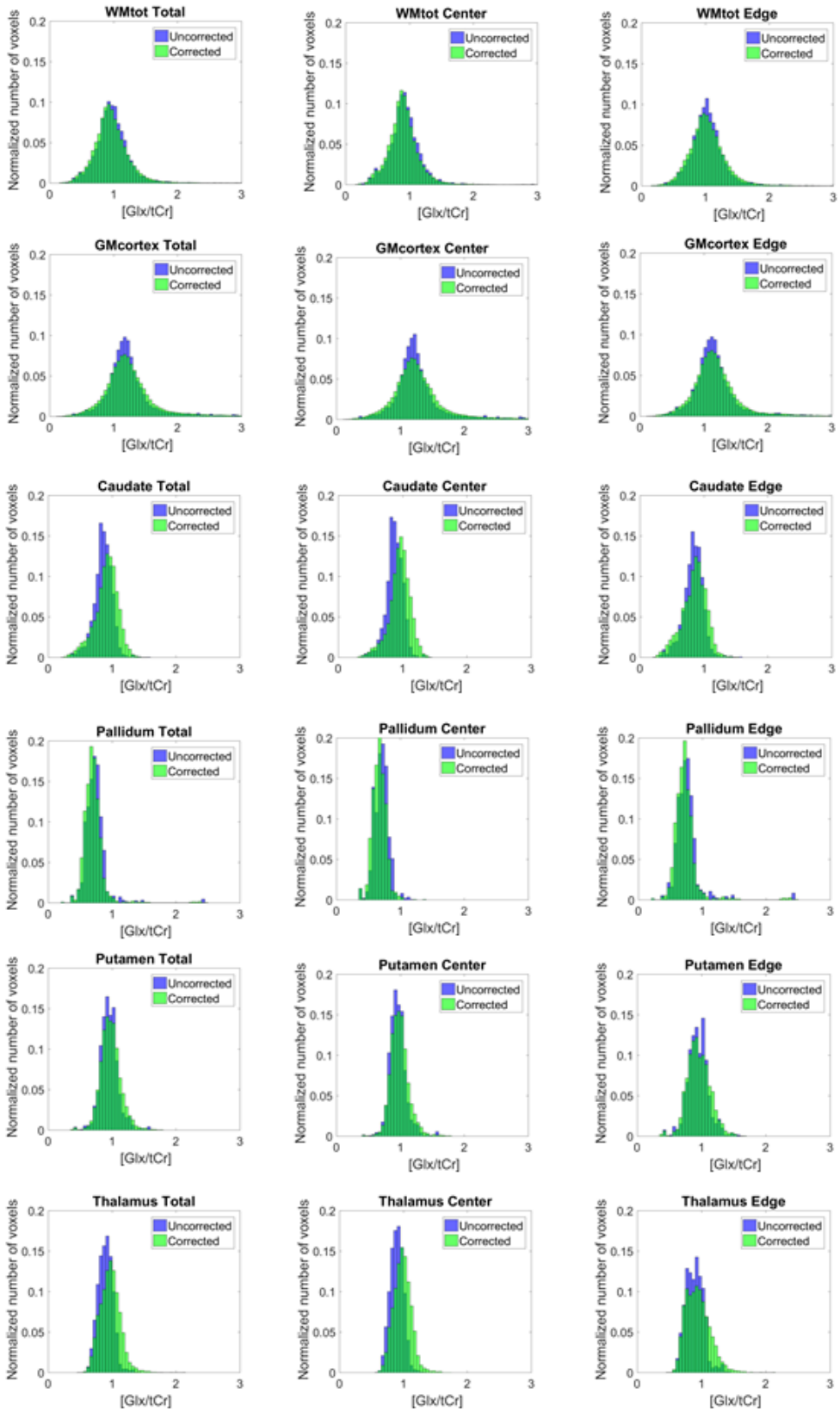

FIGURE 3.4: Normalized histograms of measured Glx/tCr concentrations of the average map before and after partial volume correction. The corrected concentrations show a larger standard deviation than the uncorrected concentrations in all histograms. The mean concentrations of the WM and pallidum are decreased and the concentrations of the caudate and thalamus, putamen and cortical GM are increased after correction. The changes are mainly happening in the center of the regions.

TABLE 3.1: Glx/tCr concentrations and standard deviations of the brain regions of the three different methods. The effect of the partial volume (PVC) and T_1 correction (T_1C) is depicted as the relative change (RC) of the mean value compared to the mean concentrations of the regions in the uncorrected maps (UC). RC is also calculated for the PVC and T_1C maps compared to the PVC maps The significance of the relative change was evaluated by the Wilcoxon signed rank test (*P<0.05, **P<0.01, ***P<0.001, including Bonferroni correction)

		UC	PVC	PVC and T_1C
WM (n=21)	Mean (sd)	0.93 (0.08)	0.91 (0.08)	0.89 (0.08)
	RC - NC		-0.02***	-0.04***
	RC - PVC			-0.02***
Cortical GM (n=17)	Mean (sd)	1.24 (0.08)	1.26 (0.08)	1.18 (0.08)
	RC - NC		0.02**	-0.05**
	RC - PVC			-0.06**
Caudate (n=17)	Mean (sd)	0.87 (0.14)	0.96 (0.17)	0.90 (0.16)
	RC - NC		0.10***	0.03*
	RC - PVC			-0.06*
Pallidum (n=10)	Mean (sd)	0.75 (0.19)	0.71 (0.18)	0.69 (0.18)
	RC - NC		-0.05*	-0.08*
	RC - PVC			-0.03*
Putamen (n=20)	Mean (sd)	0.93 (0.12)	0.96 (0.12)	0.91 (0.11)
	RC - NC		0.03***	-0.02*
	RC - PVC			-0.05*
Thalamus (n=21)	Mean (sd)	0.89 (0.11)	0.97 (0.12)	0.92 (0.11)
	RC - NC		0.09***	0.03*
	RC - PVC			-0.05***

GM and P<0.05 in the caudate, pallidum and putamen. The decrease in GM was larger than in WM.

Comparing the result of both partial volume and T_1 correction to the uncorrected regions it can be noticed that in there was a significant increase (P<0.05) in the caudate and thalamus. In the other regions there was a significant decrease of the Glx/tCr concentrations (P<0.001 in WM, P<0.01 in cortical GM and P<0.05 in the pallidum and putamen).

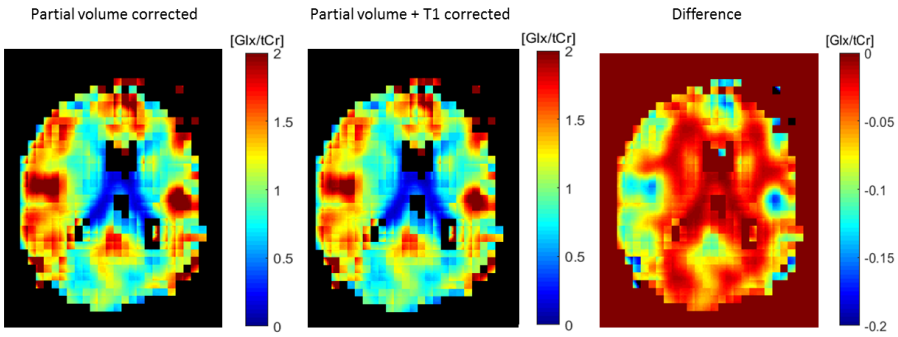

FIGURE 3.5: The effect of T_1 correction. It can be noticed that there is a decrease in Glx/tCr concentration, which is larger in GM than in WM (according to Figure 2.5).

Chapter 4

Discussion

In this study a method for partial volume correction and T_1 correction was created and implemented in the processing pipeline for 7T brain MRSI data. We found a significant difference between the Glx/tCr concentrations before and after the corrections in all regions.

4.1 Partial volume and T_1 correction

The increase in the standard deviations of the Glx/tCr concentrations after partial volume correction can be explained by the transformation of the maps into MNI space. The uncorrected maps have a lower resolution than the corrected maps. Due to upsampling the maps when they were transformed to MNI space multiple voxels have the same value. In the corrected maps the resolution is higher, which result in more variability of the voxel values in MNI space.

What can be noticed from Figure 3.4 is that the change in Glx/tCr is more obvious in most regions when only the center regions were taken into account then when the total region was used for calculation. This can be explained by the fact that using a lower threshold for selecting GM regions also some WM may be taken into account and vice versa. Therefore, it is more accurate to use the center regions instead of the total regions for calculation of the Glx/tCr concentrations.

After partial volume correction all GM regions contained higher Glx/tCr values than WM, except for the pallidum, which is also reported by Goryawala et al. [58] (see Table 4.1). Besides, the Glx/tCr concentration in the pallidum decreased after partial volume correction, in contrast with all other GM structures. This can be explained by the fact that for partial volume correction probability threshold fraction maps are created. In the pallidum region the probability values for WM were higher than for GM, which resulted in a decrease in Glx/tCr concentration after partial volume correction.

What is interesting about the partial volume and T_1 correction is that after these corrections the Glx/tCr values were lower than the values before correction in all regions, except for the caudate and the thalamus. Due to partial volume correction the concentrations in GM increased, but due to T_1 correction there was a decrease of the concentrations compared to the partial volume corrected data. In the cortical GM and putamen the decrease due to T_1 correction was larger than the increase due to partial volume correction. It can also be noticed that the increase due to partial volume correction in those regions was smaller than the increase in the caudate and the thalamus. This might be explained by the fact that during segmentation of the cortical GM and the putamen also some WM was considered to be part of those regions.

4.2 Comparison with other studies

Comparing the Glx/tCr concentrations of this study to the values reported by others, as represented in Table 4.1, it can be noticed that the values found by us are lower than most concentrations reported by others. There are several reasons that might explain this.

A possible explanation for the differences is the influence of the SNR. When the SNR level decreases, the metabolite peaks are closer to the noise level. Therefore, it is more difficult to make an accurate fit. Since the amplitudes of glutamate and glutamine are smaller than the amplitudes of creatine (see Figure 2.1), this effect is larger for these metabolites, which may result in a lower Glx/tCr ratio. The studies of Marjanska et al. [59], Kaiser et al. [60], Baker et al. [61] and Fan et al. [62] were performed using SVS, in which the number of signal averages is larger [31]. This results in a higher SNR and might explain the fact that the reported Glx/tCr concentrations are higher than the concentrations found by us. Ding et al. [63] used MRSI at a lower field strength of 3T and used a voxel size that is only a little larger than the voxel size we used, thus the data are acquired with a lower SNR [31]. This might explain the lower cortical GM Glx/tCr concentration. However, Goryawala et al. [58] and Gasparovic et al. [56] reported higher Glx/tCr concentrations although they also used 3T MRSI. This might be explained by the fact that Goryawala et al. used spectra averaged over a region of interest, and Gasparovic et al. obtained the data at a larger voxel size, both resulting in an increase of SNR [31]. The different reasons for an increase in SNR might be a reason for the higher reported Glx/tCr concentrations.

T_1 correction might also influence the difference in measured Glx/tCr concentrations. Boer et al. [41], Marjanska et al. [59], Goryawala et al. [58], Ding et al. [63] and Fan et al. [62] did not correct for this effect. The repetition times used in these studies were longer then the TR in our study and therefore the T_1 effect is lower. However, the T_1 values are 1200 and 960 seconds for GM and WM at 3T respectively [64] and 1750 and 1610 seconds at 7T [40]. This indicates that the repetition times used in these studies do not met the criterion of a TR that has to be five times longer than T_1 to acquire a fully relaxed spectrum [39]. Therefore, this might partly explain the difference in concentrations.

A third reason for the difference in in measured Glx/tCr concentrations might be the method in which partial volume correction was performed. From the studies that performed partial volume correction it is not clear if they used binary or probability maps for partial volume calculation. Using binary masks may result in larger GM tissue fractions and therefore in larger Glx/tCr concentrations in GM regions (see equation 2.2, 2.4 and 2.5).

The Glx/tCr concentration in WM reported by Boer et al.[41] is the only WM concentration of Table 4.1 that is lower than the WM concentration found by us, unless they used the same technique and voxel size. This can be explained by the fact that this value is not corrected for the partial volume effect. Presence of CSF in WM voxels might decrease the measured concentrations.

Other reasons for differences in Glx/tCr concentrations between studies may be the T_2 effect, differences in scanner, scan sequences, acquisition types, receive coils and fitting software. Due to all these influences absolute comparison between our results and the concentrations reported by others should be performed with caution. However, the differences between different studies are relatively small, and our results are within the same range as the results of other studies. Furthermore,

comparison of differences between the Glx/tCr concentrations in different brain regions is still possible.

Ordering the brain regions based on metabolite concentration, it can be noticed that after partial volume correction the pallidum has the lowest Glx/tCr concentration, followed by WM, subcortical GM nuclei except for the pallidum, and cortical GM. This is, in contrast with the uncorrected concentrations, consistent with findings of other groups as presented in Table 4.1. Based on these findings it can be concluded that the measured concentrations are more accurate after partial volume correction, enabling a more reliable comparison of Glx/tCr concentrations between patients and controls.

TABLE 4.1: Overview of Glx/tCr concentrations in different brain regions measured in vivo using ^{1}H-MRS, including scanning technique, parameters and performed corrections (relaxation and partial volume/CSF). If absolute Glu/Gln/Glx and tCr concentrations were presented, Glx/tCr concentrations were calculated and therefore standard deviations were not available. If concentrations were calculated separately for left and right or for different GM and WM regions, these concentrations were averaged. Motor cortex was compared to cortical GM, corona radiata to WM. F_{GM}: GM fraction, F_{WM}: WM fraction, TR: repetition time, TE: echo time, RC: relaxation correction, PVC: partial volume correction, scGM: subcortical GM, cGM: cortical GM.

[Glx/tCr]	**Region** (F_{GM}/F_{WM})	**Technique**	**TR/TE (ms)**	**Voxel size (mm^3)**	**RC**	**PVC**	**Reference**
0.56 1.14	WM scGM	7T MRSI	1000/1.41	5×5×10	-	-	Boer et al., 2011 [41]
1.16 1.04	motor cortex (0.73/0.19) basal ganglia (0.73/0.25)	7T SVS	4500/35	20×20×20 15×40×15	-	CSF	Marjanska et al., 2012[59]
1.04 1.38	corona radiata motor cortex	4T SVS	2000/15	20×20×20 20×20×20	T1	PVC	Kaiser et al., 2005 [60]
1.07 1.28 1.09 (0.17) 1.01 (0.14) 1.20 (0.84) 1.07 (0.14)	mean WM mean cGM caudate pallidum putamen thalamus	3T MRSI	1551/17.6	5.6×5.6×10	-	-	Goryawala et al., 2016 [58]
0.96 1.06	mean WM mean cGM	3T MRSI	1550/17.6	5.6×5.6×10	-	PVC	Ding et al., 2015 [63]
1.16 1.63	WM scGM	3T MRSI	1500/40	6.9×6.9×15	T1, T2	PVC	Gasparovic et al., 2011 [56]
1.08 1.31 1.12	mean WM mean cGM thalamus	3T SVS	2000/35	20×20×20 20×20×20 20×20×20	T1, T2	CSF	Baker et al., 2008 [61]
1.90	thalamus	3T SVS	3000/35	16×28×16	-	PVC	Fan et. al., 2017 [62]

4.3 Limitations

Partial volume correction was based on a comparison between the T_1 and MRSI data, resulting in a corrected metabolite map with a resolution of 1x1x1 mm^3. To obtain this corrected map, it was assumed that the signal of the anatomical and MRSI data are acquired from exactly the same position. However, there are two aspects that caused a position difference between the anatomical and MRSI data.

Firstly, since the scan protocol lasts about 50 minutes, there is a reasonable chance that the subject has moved between the anatomical and MRSI data acquisition. Because of the use of a crusher coil during the acquisition of all data, the space to move is reduced. Nonetheless, a movement of the subject larger than 1 mm is still possible. Besides, the crusher coil moves during acquisition of the MRSI data, causing ticking against the head of the subject. This can provoke the subject to move as well. When a new crusher coil will be developed it is recommended to further reduce the space within the crusher coil. Another suggestion is to create a soft layer between the front of the crusher coil and the forehead of the subject to reduce the ticking, resulting in less movement of the subject.

Secondly, the calculated fraction maps used for partial volume correction were based on segmentation in MNI space, to eliminate bad GM/WM segmentation due to scan artifacts that occurs in some of the subjects. A consequence of this method is that the fraction maps have to be transformed from MNI space to the 2D slice. The nonlinear transformation matrix may contain an offset of a couple of millimeters, resulting in fraction maps that not fully align with the anatomical map. Since the correction was based on a resolution of 1x1x1 mm, this can influence the partial volume correction. In the current study the influence of the alignment error was reduced by calculating the Glx/tCr concentrations in only the center part of the regions. However, for a more accurate calculation of the fraction maps it is recommended to perform the calculations in the subject space and only use the MNI fraction maps in the subjects in which segmentation in the 2D slice fails.

4.4 Future directions

4.4.1 Evaluation of partial volume and T_1 correction

Based on comparison of the corrected maps to the anatomical maps and comparison of the calculated concentrations with literature it is suggested that partial volume and T_1 correction result in more reliable Glx/tCr concentrations. However, because the actual glutamate, glutamine and creatine concentrations per region were not known, it could not be confirmed if the corrected concentrations are closer to the actual concentration. To validate the effect of the corrections, it is recommended to create a virtual phantom with an anatomical and MRSI slice of the brain in which the metabolite concentrations are known. After addition of noise this phantom can be used to perform partial volume and T_1 correction. By calculating the metabolite concentrations per brain region in this phantom before and after the corrections and compare both results to the known concentrations, it can be validated if partial volume and T_1 correction result in more accurate calculations of Glx/tCr concentrations.

4.4.2 Comparison between patients and controls

Looking at the absolute change between the partial volume and T_1 corrected and uncorrected Glx/tCr concentrations these changes vary from -0.06 in the pallidum to +0.03 in the caudate and thalamus (see Table 3.1). Comparing these values to studies evaluating the glutamate concentration in schizophrenia patients and healthy control subjects using 7T MRI, there is one study that reported a significant difference in glutamate concentration between those groups, and also reported values of tCr [4]. The Glx/tCr concentration in the anterior cingulate cortex was 0.08 lower in schizophrenia patients. This value is close to the range of the absolute differences

with and without correction we found. Therefore, it is expected that partial volume and T_1 correction may have an added value in the comparison of Glx/tCr concentrations between patients who experience a psychosis and healthy control subjects. To evaluate if this is the case, it is recommended to calculate the Glx/tCr per region for both the uncorrected and corrected concentrations, and compare the differences between patients and controls with and without the corrections.

In this study the Glx/tCr concentrations were calculated for the total WM and cortical GM region. However, studies that compared differences in glutamate concentration between patients and controls reported significant differences in smaller regions, as shown in Table 4.2. Because these studies used SVS, it is not known if these differences were specific for those regions. Nonetheless, Goryawala et al. [58], Ding et al. [63] and Baker et al. [61] already showed that there are regional differences in WM and cortical GM. When the concentrations within a large region are calculated, it might be possible that regional differences between patients and controls cannot be noticed anymore because concentrations are averaged. Therefore, it is recommended to split WM and cortical GM into smaller regions when patients and controls are compared.

TABLE 4.2: Overview of MRS studies on the glutamate concentrations of patients with psychotic disorders compared to healthy control subjects. FEP: first episode psychosis, SCZ: schizophrenia, SAD: schizoaffective disorder, MI: medication naïve, MF: medication free ACC: anterior cingulate cortex, MFC: medial frontal cortex, OC = occipital cortex, BG: basal, Glu: glutamate, Gln: glutamine, Glx: glutamate + glutamine

Population	**Region**						**Technique**	**Reference**
	ACC	**MFC**	**OC**	**BG**	**MTL**	**FWM**		
FEP	Glu ↓						7T SVS	Reid et al., 2019 [4]
FEP	Glu ↓						7T SVS	Wang et al., 2019 [5]
SCZ/SAD	Glu ↓						7T SVS	Kumar et al., 2018 [6]
SCZ			Glu ↓				7T SVS	Thakkar et al., 2017 [7]
SCZ/SAD	$\frac{Gln}{Glu}$ ↑						7T SVS	Rowland et al., 2016 [8]
SCZ/SAD - age 40	Glu ↑						7T SVS	Brandt et al., 2016 [9]
SCZ - MI/MF		Glu ↑		Glu ↑			1.5T, 3T, 4T SVS	Poels et al., 2014 (review) [11]
FEP				Glx ↑	Glx ↑		1.5T, 3T, 4T SVS	Merritt et al., 2016 (review) [12]
SCZ				Glx ↑	Glx ↑	Glx ↑		
SCZ		Glu ↓					1.5T, 3T, 4T SVS	Marsman et al., 2013 (review) [13]

The Glx/tCr concentrations of healthy control subjects were calculated by thresholding brain region masks based on visual interpretation and averaging all values within these regions. There are two consequences of this method. First of all, it was assumed that the region masks are a good representation of the brain regions. However, as can be noticed in Figure 2.8, these region masks do not perfectly align with the anatomy, especially in the WM and cortical GM regions. It was decided to take into account only the center regions in order to prevent the influence of surrounding tissue as much as possible, but the consequence of this is that some parts of the regions that belong to that specific region were not taken into account. Besides, it

was assumed that the Glx/tCr concentrations are equal throughout a specific brain region. However, this does not have to be the case. Therefore, it is recommended to also perform voxel wise instead of region wise comparison in evaluation of the differences in Glx/tCr concentrations between patients and controls, in order to get rid of the influence of the region masks and the assumption that the metabolite concentrations are equal within the selected brain regions.

4.4.3 GM and WM concentrations

The GM and WM concentrations used for partial volume correction were calculated from all GM an WM voxels within one subject. However, Sailasuta et al. [65] showed that the concentration of the metabolites glutamate and creatine differs significantly between brain regions. Due to the limited number of MRSI voxels within one brain region it was not possible to calculate specific GM and WM values per region within one subject. Calculation of average regional values between different subject may overcome this problem. However, because the number of data sets obtained during this study is relatively small, averaging of regional values between this number of subjects would result in unreliable values. Moreover, metabolite concentrations are influenced by age and gender [65]. To obtain more accurate regional GM and WM values per subject, a healthy control reference atlas specific for a certain age range and gender can be used [66].

4.4.4 Absolute concentrations

The calculated metabolite concentrations were all denoted with tCr as scaling factor, assuming that this metabolite is homogeneously distributed in brain. However, Sailasuta et al. [65] demonstrated that there are significant regional differences in tCr concentration between brain regions. Calculation of absolute metabolite concentrations can overcome this problem. To enable this, the data has to be corrected for B_1 inhomogeneities that cause large spatial variations in signal [48]. This can be performed by post processing of the data using $B_1{}^+$ maps. It is recommended to add this acquisition to the scanning protocol to enable calculation of absolute metabolite concentrations.

4.5 Conclusion

Partial volume and T_1 correction resulted in significantly different Glx/tCr concentrations compared to the concentrations before correction in all evaluated regions. Based on the comparison with literature it is suggested that the corrections result in a more accurate calculation of Glx/tCr concentrations. To validate this, it is recommended to compare the uncorrected and corrected maps to a phantom with known Glx/tCr concentrations.

It has to be evaluated if partial volume and T_1 correction result in a more accurate comparison Glx/tCr concentrations between patients who experienced a psychosis and healthy control subjects.

Bibliography

[1] W. Rössler, H. Joachim Salize, J. van Os, and A. Riecher-Rössler, "Size of burden of schizophrenia and psychotic disorders", *European Neuropsychopharmacology*, vol. 15, no. 4, pp. 399–409, 2005, ISSN: 0924-977X. DOI: 10.1016/J.EURONEURO.2005.04.009.

[2] J. T. Coyle, "NMDA Receptor and Schizophrenia: A Brief History", *Schizophrenia Bulletin*, vol. 38, no. 5, pp. 920–926, 2012. DOI: 10.1093/schbul/sbs076.

[3] O. Howes, R. McCutcheon, and J. Stone, "Glutamate and dopamine in schizophrenia: An update for the 21 st century", *Journal of Psychopharmacology*, vol. 29, no. 2, pp. 97–115, 2015, ISSN: 0269-8811. DOI: 10.1177/0269881114563634.

[4] M. A. Reid, N. Salibi, D. M. White, T. J. Gawne, T. S. Denney, and A. C. Lahti, "7T Proton Magnetic Resonance Spectroscopy of the Anterior Cingulate Cortex in First-Episode Schizophrenia", *Schizophrenia Bulletin*, vol. 45, no. 1, pp. 180–189, 2019, ISSN: 0586-7614. DOI: 10.1093/schbul/sbx190.

[5] A. M. Wang, S. Pradhan, J. M. Coughlin, A. Trivedi, S. L. DuBois, J. L. Crawford, T. W. Sedlak, F. C. Nucifora, G. Nestadt, L. G. Nucifora, D. J. Schretlen, A. Sawa, and P. B. Barker, "Assessing Brain Metabolism With 7-T Proton Magnetic Resonance Spectroscopy in Patients With First-Episode Psychosis", *JAMA Psychiatry*, 2019, ISSN: 2168-622X. DOI: 10.1001/jamapsychiatry.2018.3637.

[6] J. Kumar, E. B. Liddle, C. C. Fernandes, L. Palaniyappan, E. L. Hall, S. E. Robson, M. Simmonite, J. Fiesal, M. Z. Katshu, A. Qureshi, M. Skelton, N. G. Christodoulou, M. J. Brookes, P. G. Morris, and P. F. Liddle, "Glutathione and glutamate in schizophrenia: a 7T MRS study", *Molecular Psychiatry*, p. 1, 2018, ISSN: 1359-4184. DOI: 10.1038/s41380-018-0104-7.

[7] K. N. Thakkar, L. Rösler, J. P. Wijnen, V. O. Boer, D. W. Klomp, W. Cahn, R. S. Kahn, and S. F. Neggers, "7T Proton Magnetic Resonance Spectroscopy of Gamma-Aminobutyric Acid, Glutamate, and Glutamine Reveals Altered Concentrations in Patients With Schizophrenia and Healthy Siblings", *Biological Psychiatry*, vol. 81, no. 6, pp. 525–535, 2017, ISSN: 0006-3223. DOI: 10.1016/J.BIOPSYCH.2016.04.007.

[8] L. M. Rowland, S Pradhan, S Korenic, S. A. Wijtenburg, L. E. Hong, R. A. Edden, and P. B. Barker, "Elevated brain lactate in schizophrenia: a 7T magnetic resonance spectroscopy study.", *Translational psychiatry*, vol. 6, no. 11, e967, 2016, ISSN: 2158-3188. DOI: 10.1038/tp.2016.239.

[9] A. S. Brandt, P. G. Unschuld, S. Pradhan, I. A. L. Lim, G. Churchill, A. D. Harris, J. Hua, P. B. Barker, C. A. Ross, P. C. M. van Zijl, R. A. E. Edden, and R. L. Margolis, "Age-related changes in anterior cingulate cortex glutamate in schizophrenia: A (1)H MRS Study at 7 Tesla.", *Schizophrenia research*, vol. 172, no. 1-3, pp. 101–5, 2016, ISSN: 1573-2509. DOI: 10.1016/j.schres.2016.02.017.

[10] L. Tebartz van Elst, G. Valerius, M. Büchert, T. Thiel, N. Rüsch, E. Bubl, J. Hennig, D. Ebert, and H. M. Olbrich, "Increased Prefrontal and Hippocampal Glutamate Concentration in Schizophrenia: Evidence from a Magnetic Resonance Spectroscopy Study", *Biological Psychiatry*, vol. 58, no. 9, pp. 724–730, 2005, ISSN: 0006-3223. DOI: 10.1016/J.BIOPSYCH.2005.04.041.

[11] E. M. Poels, L. S. Kegeles, J. T. Kantrowitz, D. C. Javitt, J. A. Lieberman, A. Abi-Dargham, and R. R. Girgis, "Glutamatergic abnormalities in schizophrenia: A review of proton MRS findings", *Schizophrenia Research*, vol. 152, no. 2-3, pp. 325–332, 2014, ISSN: 0920-9964. DOI: 10.1016/J.SCHRES.2013.12.013.

[12] K. Merritt, A. Egerton, M. J. Kempton, M. J. Taylor, and P. K. McGuire, "Nature of Glutamate Alterations in Schizophrenia", *JAMA Psychiatry*, vol. 73, no. 7, p. 665, 2016, ISSN: 2168-622X. DOI: 10.1001/jamapsychiatry.2016.0442.

[13] A. Marsman, M. P. Van Den Heuvel, D. W. J. Klomp, R. S. Kahn, P. R. Luijten, and H. E. Hulshoff Pol, "Glutamate in Schizophrenia: A Focused Review and Meta-Analysis of 1 H-MRS Studies", *Schizophrenia Bulletin*, vol. 39, no. 1, pp. 120–129, 2013. DOI: 10.1093/schbul/sbr069.

[14] D. B. Arciniegas, "Psychosis", *CONTINUUM: Lifelong Learning in Neurology*, vol. 21, no. 3 Behavioral Neurology and Neuropsychiatry, pp. 715–736, 2015, ISSN: 1080-2371. DOI: 10.1212/01.CON.0000466662.89908.e7.

[15] J. van Os and S. Kapur, "Schizophrenia", *The Lancet*, vol. 374, no. 9690, pp. 635–645, 2009, ISSN: 01406736. DOI: 10.1016/S0140-6736(09)60995-8.

[16] R. A. Knight, "Relating cognitive processes to symptoms: a strategy to counter methodological difficulties", in *Positive and Negative Symptoms in Psychosis: Description, Research and Future Directions*, Lawrence Elrbaum Associates, Publishers, 1987, ch. 1, ISBN: 0-89859-880-X.

[17] J. Perälä, J. Suvisaari, S. I. Saarni, K. Kuoppasalmi, E. Isometsä, S. Pirkola, T. Partonen, A. Tuulio-Henriksson, J. Hintikka, T. Kieseppä, T. Härkänen, S. Koskinen, and J. Lönnqvist, "Lifetime Prevalence of Psychotic and Bipolar I Disorders in a General Population", *Archives of General Psychiatry*, vol. 64, no. 1, p. 19, 2007, ISSN: 0003-990X. DOI: 10.1001/archpsyc.64.1.19.

[18] C. Forray and R. Buller, "Challenges and opportunities for the development of new antipsychotic drugs", *Biochemical Pharmacology*, vol. 143, pp. 10–24, 2017, ISSN: 00062952. DOI: 10.1016/j.bcp.2017.05.009.

[19] S. Kapur, "Psychosis as a state of aberrant salience: A framework linking biology, phenomenology, and pharmacology in schizophrenia", *American Journal of Psychiatry*, vol. 160, no. 1, pp. 13–23, 2003, ISSN: 0002953X. DOI: 10.1176/appi.ajp.160.1.13.

[20] J. P. Roiser, O. D. Howes, C. A. Chaddock, E. M. Joyce, and P. McGuire, "Neural and behavioral correlates of aberrant salience in individuals at risk for psychosis.", *Schizophrenia bulletin*, vol. 39, no. 6, pp. 1328–36, 2013, ISSN: 1745-1701. DOI: 10.1093/schbul/sbs147.

[21] S. Kapur, O. Agid, R. Mizrahi, and M. Li, "How antipsychotics work - From receptors to reality", *NeuroRx*, vol. 3, no. 1, pp. 10–21, 2006, ISSN: 15455351. DOI: 10.1016/j.nurx.2005.12.003.

[22] M Laruelle, "Imaging dopamine transmission in schizophrenia. A review and meta-analysis.", *The quarterly journal of nuclear medicine : Official publication of the Italian Association of Nuclear Medicine (AIMN) [and] the International Association of Radiopharmacology (IAR)*, vol. 42, no. 3, pp. 211–21, 1998, ISSN: 1125-0135.

[23] O. Guillin, A. Abi-Dargham, and M. Laruelle, "Neurobiology of Dopamine in Schizophrenia", *International Review of Neurobiology*, vol. 78, pp. 1–39, 2007, ISSN: 0074-7742. DOI: 10.1016/S0074-7742(06)78001-1.

[24] Á. Del Rey-Mejías, D. Fraguas, C. M. Díaz-Caneja, L. Pina-Camacho, J. Castro-Fornieles, I. Baeza, A. Espliego, J. Merchán-Naranjo, A. González-Pinto, E. de la Serna, B. Payá, M. Graell, C. Arango, and M. Parellada, "Functional deterioration from the premorbid period to 2 years after the first episode of psychosis in early-onset psychosis", *European Child & Adolescent Psychiatry*, vol. 24, no. 12, pp. 1447–1459, 2015, ISSN: 1018-8827. DOI: 10.1007/s00787-015-0693-5.

[25] D. Kondziella, E. Brenner, E. M. Eyjolfsson, and U. Sonnewald, "How do glial–neuronal interactions fit into current neurotransmitter hypotheses of schizophrenia?", *Neurochemistry International*, vol. 50, no. 2, pp. 291–301, 2007, ISSN: 0197-0186. DOI: 10.1016/J.NEUINT.2006.09.006.

[26] J. M. Stone, P. D. Morrison, and L. S. Pilowsky, "Glutamate and dopamine dysregulation in schizophrenia-a synthesis and selective review", *J Psychopharm Journal of Psychopharmacology*, vol. 21, no. 4, pp. 440–452, 2007, ISSN: 0269-8811. DOI: 10.1177/0269881106073126.

[27] S. Cull-Candy, S. Brickley, and M. Farrant, "NMDA receptor subunits: Diversity, development and disease", *Current Opinion in Neurobiology*, vol. 11, no. 3, pp. 327–335, 2001, ISSN: 09594388. DOI: 10.1016/S0959-4388(00)00215-4.

[28] J. W. Olney and N. B. Farber, "Glutamate Receptor Dysfunction and Schizophrenia", *Archives of General Psychiatry Psychiatry*, vol. 52, pp. 998–1007, 1995.

[29] J. T. Bushberg, J. A. Seibert, E. M. Leidholdt, and J. M. Boone, *The essential physics of medical imaging*, Third edit. Lippincott Williams & Wilkins, 2011, p. 1030, ISBN: 9780781780575.

[30] K. M. Cecil, "Proton Magnetic Resonance Spectroscopy: Technique for the Neuroradiologist", *Neuroimaging clinics of North America*, vol. 23, no. 3, p. 381, 2013, ISSN: 1557-9867. DOI: 10.1016/J.NIC.2012.10.003.

[31] D. W. McRobbie, E. A. Moore, M. J. Graves, and M. R. Prince, *MRI From Picture to Proton*, 2nd ed. Cambridge: Cambridge University Press, 2006.

[32] *Single vs Multi-Voxel - Questions and Answers in MRI*. [Online]. Available: http://mriquestions.com/single-v-multi-voxel.html (visited on 08/12/2019).

[33] M. D. Rubio, J. B. Drummond, and J. H. Meador-Woodruff, "Glutamate receptor abnormalities in schizophrenia: implications for innovative treatments.", *Biomolecules & therapeutics*, vol. 20, no. 1, pp. 1–18, 2012, ISSN: 1976-9148. DOI: 10.4062/biomolther.2012.20.1.001.

[34] R. Shafee, R. L. Buckner, and B. Fischl, "Gray matter myelination of 1555 human brains using partial volume corrected MRI images", *NeuroImage*, vol. 105, pp. 473–485, 2015, ISSN: 1053-8119. DOI: 10.1016/J.NEUROIMAGE.2014.10.054.

[35] R. A. de Graaf, "Spectroscopic Imaging and Multivolume Localization", in *In vivo NMR Spectroscopy - 2nd Edition: Principles and Techniques*, 2nd ed., John Wiley & Sons, Ltd, 2007, ch. 7, pp. 354–356, ISBN: 978-0470-026700.

[36] T. Kirchner, A. Fillmer, J. Tsao, K. P. Pruessmann, and A. Henning, "Reduction of voxel bleeding in highly accelerated parallel 1H MRSI by direct control of the spatial response function", *Magnetic Resonance in Medicine*, vol. 73, no. 2, pp. 469–480, 2015, ISSN: 15222594. DOI: 10.1002/mrm.25185.

[37] V. O. Boer, T. Van De Lindt, P. R. Luijten, and D. W. J. Klomp, "Lipid suppression for brain MRI and MRSI by means of a dedicated crusher coil", *Magnetic Resonance in Medicine*, vol. 73, no. 6, pp. 2062–2068, 2015, ISSN: 15222594. DOI: 10.1002/mrm.25331.

[38] W. Weber-Fahr, G. Ende, D. F. Braus, P. Bachert, B. J. Soher, F. A. Henn, and C. Büchel, "A fully automated method for tissue segmentation and CSF-correction of proton MRSI metabolites corroborates abnormal hippocampal NAA in schizophrenia", *NeuroImage*, vol. 16, no. 1, pp. 49–60, 2002, ISSN: 10538119. DOI: 10.1006/nimg.2002.1057.

[39] J. F. A. Jansen, W. H. Backes, K. Nicolay, and M. E. Kooi, "H MR Spectroscopy of the Brain: Absolute Quantification of Metabolites", *Radiology*, vol. 240, no. 2, 2006. DOI: 10.1148/radiol.2402050314.

[40] L. Xin, B. Schaller, V. Mlynarik, H. Lu, and R. Gruetter, "Proton T1 relaxation times of metabolites in human occipital white and gray matter at 7 T", *Magnetic Resonance in Medicine*, vol. 69, no. 4, pp. 931–936, 2013, ISSN: 07403194. DOI: 10.1002/mrm.24352.

[41] V. O. Boer, J. C. Siero, H. Hoogduin, J. S. van Gorp, P. R. Luijten, and D. W. Klomp, "High-field MRS of the human brain at short TE and TR", *NMR in Biomedicine*, vol. 24, no. 9, pp. 1081–1088, 2011, ISSN: 09523480. DOI: 10.1002/nbm.1660.

[42] J. Ma, C. Wismans, Z. Cao, D. W. J. Klomp, J. P. Wijnen, and W. A. Grissom, "Tailored spiral in-out spectral-spatial water suppression pulses for magnetic resonance spectroscopic imaging", *Magnetic Resonance in Medicine*, vol. 79, no. 1, pp. 31–40, 2018, ISSN: 07403194. DOI: 10.1002/mrm.26683.

[43] S. Nassirpour, P. Chang, and A. Henning, "High and ultra-high resolution metabolite mapping of the human brain using 1H FID MRSI at 9.4T", *NeuroImage*, vol. 168, pp. 211–221, 2018, ISSN: 1053-8119. DOI: 10.1016/J.NEUROIMAGE.2016.12.065.

[44] T. Kirchner, A. Fillmer, and A. Henning, "Mechanisms of SNR and line shape improvement by B0 correction in overdiscrete MRSI reconstruction", *Magnetic Resonance in Medicine*, vol. 77, no. 1, pp. 44–56, 2017, ISSN: 15222594. DOI: 10.1002/mrm.26118.

[45] A. Henning, A. Fuchs, J. B. Murdoch, and P. Boesiger, "Slice-selective FID acquisition, localized by outer volume suppression (FIDLOVS) for 1H-MRSI of the human brain at 7 T with minimal signal loss", *NMR in Biomedicine*, vol. 22, no. 7, pp. 683–696, 2009, ISSN: 09523480. DOI: 10.1002/nbm.1366.

[46] U Klose, "In vivo proton spectroscopy in presence of eddy currents", *Magnetic Resonance in Medicine*, vol. 14, no. 1, pp. 26–30, 1990, ISSN: 0740-3194.

[47] S. W. Provencher, "Estimation of Metabolite Concentrations from Localized in Vivo Proton NMR Spectra", *Magnetic Resonance in Medicine*, vol. 30, pp. 672–679, 1993.

[48] W Bogner, S Gruber, S Trattnig, and M Chmelik, "High-resolution mapping of human brain metabolites by free induction decay 1 H MRSI at 7 T", 2011. DOI: 10.1002/nbm.1805.

[49] M. Jenkinson, P. Bannister, M. Brady, and S. Smith, "Improved Optimization for the Robust and Accurate Linear Registration and Motion Correction of Brain Images", 2002. DOI: 10.1006/nimg.2002.1132.

[50] J. L. R. Andersson, M. Jenkinson, and S. Smith, "Non-linear registration aka Spatial normalisation FMRIB Technial Report TR07JA2", Tech. Rep., 2007.

[51] Y. Zhang, M. Brady, and S. Smith, "Segmentation of brain MR images through a hidden Markov random field model and the expectation-maximization algorithm", *IEEE Transactions on Medical Imaging*, vol. 20, no. 1, pp. 45–57, 2001, ISSN: 02780062. DOI: 10.1109/42.906424.

[52] K. Hashimoto, G. Engberg, E. Shimizu, C. Nordin, L. H. Lindström, and M. Iyo, "Elevated glutamine/glutamate ratio in cerebrospinal fluid of first episode and drug naive schizophrenic patients.", *BMC psychiatry*, vol. 5, p. 6, 2005, ISSN: 1471-244X. DOI: 10.1186/1471-244X-5-6.

[53] F. Schubert, J. Gallinat, F. Seifert, and H. Rinneberg, "Glutamate concentrations in human brain using single voxel proton magnetic resonance spectroscopy at 3 Tesla", *NeuroImage*, vol. 21, no. 4, pp. 1762–1771, 2004, ISSN: 10538119. DOI: 10.1016/j.neuroimage.2003.11.014.

[54] Y. Zhang and J. Shen, "Regional and tissue-specific differences in brain glutamate concentration measured by in vivo single voxel MRS", *Journal of Neuroscience Methods*, vol. 239, pp. 94–99, 2015, ISSN: 0165-0270. DOI: 10.1016/J.JNEUMETH.2014.09.021.

[55] H. P. Hetherington, J. W. Pan, G. F. Mason, D. Adams, M. J. Vaughn, D. B. Twie, and G. M. Pohost, "Quantitative 1H Spectroscopic Imaging of Human Brain at 4.1 T Using Image Segmentation Hoby", *Magnetic resonance in medicine*, vol. 36, no. 1, pp. 21–29, 1996, ISSN: 07403194. DOI: 10.1016/B978-1-85617-653-8.00002-8. arXiv: arXiv:1308.3139v1.

[56] C. Gasparovic, E. J. Bedrick, A. R. Mayer, R. A. Yeo, H. Chen, E. Damaraju, V. D. Calhoun, and R. E. Jung, "Test-retest reliability and reproducibility of short-echo-time spectroscopic imaging of human brain at 3T.", *Magnetic resonance in medicine*, vol. 66, no. 2, pp. 324–32, 2011, ISSN: 1522-2594. DOI: 10.1002/mrm.22858.

[57] J. Mazziotta, A. Toga, A. Evans, P. Fox, J. Lancaster, K. Zilles, R. Woods, T. Paus, G. Simpson, B. Pike, C. Holmes, L. Collins, P. Thompson, D. MacDonald, M. Iacoboni, T. Schormann, K. Amunts, N. Palomero-Gallagher, S. Geyer, L. Parsons, K. Narr, N. Kabani, G. L. Goualher, D. Boomsma, T. Cannon, R. Kawashima, and B. Mazoyer, "A probabilistic atlas and reference system for the human brain: International Consortium for Brain Mapping (ICBM)", *Philosophical Transactions of the Royal Society of London. Series B: Biological Sciences*, vol. 356, no. 1412, R. Kötter, Ed., pp. 1293–1322, 2001, ISSN: 0962-8436. DOI: 10.1098/rstb.2001.0915.

[58] M. Z. Goryawala, S. Sheriff, and A. A. Maudsley, "Regional distributions of brain glutamate and glutamine in normal subjects", *NMR in Biomedicine*, vol. 29, no. 8, pp. 1108–1116, 2016, ISSN: 10991492. DOI: 10.1002/nbm.3575.

[59] M. Marjańska, E. J. Auerbach, R. Valabrègue, P.-F. Van de Moortele, G. Adriany, and M. Garwood, "Localized 1H NMR spectroscopy in different regions of human brain in vivo at 7 T: T2 relaxation times and concentrations of cerebral metabolites", *NMR in Biomedicine*, vol. 25, no. 2, pp. 332–339, 2012, ISSN: 09523480. DOI: 10.1002/nbm.1754.

[60] L. G. Kaiser, N. Schuff, N. Cashdollar, and M. W. Weiner, "Age-related glutamate and glutamine concentration changes in normal human brain: 1 H MR spectroscopy study at 4 T", *Neurobiology of Aging*, vol. 26, pp. 665–672, 2005. DOI: 10.1016/j.neurobiolaging.2004.07.001.

[61] E. H. Baker, G. Basso, P. B. Barker, M. A. Smith, D. Bonekamp, and A. Horská, "Regional apparent metabolite concentrations in young adult brain measured by1H MR spectroscopy at 3 Tesla", *Journal of Magnetic Resonance Imaging*, vol. 27, no. 3, pp. 489–499, 2008, ISSN: 10531807. DOI: 10.1002/jmri.21285.

[62] S. Fan, D. C. Cath, O. A. van den Heuvel, Y. D. van der Werf, C. Schöls, D. J. Veltman, and P. J. Pouwels, "Abnormalities in metabolite concentrations in tourette's disorder and obsessive-compulsive disorder—A proton magnetic resonance spectroscopy study", *Psychoneuroendocrinology*, vol. 77, pp. 211–217, 2017, ISSN: 03064530. DOI: 10.1016/j.psyneuen.2016.12.007.

[63] X.-Q. Ding, A. A. Maudsley, M. Sabati, S. Sheriff, P. R. Dellani, and H. Lanfermann, "Reproducibility and reliability of short-TE whole-brain MR spectroscopic imaging of human brain at 3T", *Magnetic Resonance in Medicine*, vol. 73, no. 3, pp. 921–928, 2015, ISSN: 07403194. DOI: 10.1002/mrm.25208.

[64] V. Mlynrik, S. Gruber, and E. Moser, "Proton T1 and T2 relaxation times of human brain metabolites at 3 Tesla", *NMR in Biomedicine*, vol. 14, no. 5, pp. 325–331, 2001, ISSN: 09523480. DOI: 10.1002/nbm.713.

[65] N. Sailasuta, T. Ernst, and L. Chang, "Regional variations and the effects of age and gender on glutamate concentrations in the human brain ", 2007. DOI: 10.1016/j.mri.2007.06.007. [Online]. Available: https://www.ncbi.nlm.nih.gov/pmc/articles/PMC2712610/pdf/nihms107613.pdf.

[66] A. Bhogal, T. A. Broeders, M. Edens, S. Nassirpour, P. Chang, P. R. Luijten, D. Klomp, H. Vinkers, Christiaan, and J. P. Wijnen, "Detailed in vivo brain atlas of metabolic and macromolecular distributions in humans using 7-T 1H Magnetic Resonance Spectroscopic Imaging", *Unpublished*, 2018.

[67] R. E. Gordon and W. E. Timms, "Magnet systems used in medical NMR", *Computerized Radiology*, vol. 8, no. 5, pp. 245–261, 1984.

[68] R. A. de Graaf, "Basic principles", in *In vivo NMR Spectroscopy - 2nd Edition: Principles and Techniques*, 2007, ch. 1, pp. 1–41, ISBN: 978-0470-26700.

[69] F. A. Bovey, "Fundamental principles", in *Nuclear Magnetic Resonance Spectroscopy*, 1988, ch. 1, pp. 1–36, ISBN: 0-12-119752-2.

[70] R. A. de Graaf, "In vivo NMR Spectroscopy - Static Aspects", in *In vivo NMR Spectroscopy - 2nd Edition: Principles and Techniques*, John Wiley & Sons, Ltd., 2007, ch. 2, pp. 43–95, ISBN: 978-0470-026700.

Appendix A

Magnetic resonance spectroscopy

Magnetic resonance spectroscopy (MRS) is a technique based on in vivo nuclear magnetic resonance (NMR) [67]. It reconstructs a spectrum based on specific resonance frequencies of nuclear spins of different molecules dissolved in the intra and extra-cellular space.

When a nucleus (in common ^{1}H MRS) is placed in a magnetic field it acts as a small dipole and will align with the main magnetic field. The magnetic moment of the nucleus precesses (spins) about the magnetic field. The resonance frequency of a particular nucleus depends on the chemical structure of the molecule to which it is bonded. The ^{1}H nucleus is shielded from the external magnetic field B_0 by the electrons around it and those belonging to neighboring atoms, which results in a reduced magnetic field. The effective local magnetic field B_L at the nucleus will be:

$$B_L = B_0(1 - \sigma) \tag{A.1}$$

with σ the shielding constant which depends on the chemical environment of the nucleus, expressed in parts per million (ppm). ^{1}H nuclei in molecules with a different chemical environment have different shielding constants which changes B_L. According to equation A.2, a difference in B_L leads to a difference in local resonance frequency v_L, depending on the chemical environment of the nucleus.

$$v_L = \frac{\gamma}{2\pi} B_L \tag{A.2}$$

In this equation γ is the gyromagnetic ratio, which is specific for a certain nucleus. The difference in Larmor frequency v_L results in a chemical shift of the nucleus from the frequency of a chemically inert reference molecule v_{ref}. Chemical shift δ, expressed in terms of ppm, is defined as

$$\delta = \frac{v_L - v_{ref}}{v_{ref}} \cdot 10^6 \tag{A.3}$$

The chemical shifts can be depicted in a ^{1}H NMR spectrum, from which an example is given in figure 1 [67], [68].

The differences in resonance frequency due to the chemical shifts are very small because of the small variation in shielding constants [67]. Shielding is proportional to the applied magnetic field B_0 which means that a high magnetic field leads to a larger chemical shift dispersion (see equation A.1 and A.2). This allows for easier distinction between different resonance signals [69]. Another advantage of the use of a high magnetic field is a better signal to noise ratio (SNR) compared to lower magnetic fields [45]. These properties are useful in research into glutamate, because the chemical structure of glutamate is similar to that of glutamine (which is synthesized from glutamate) and therefore the resonance signals of glutamate and glutamine

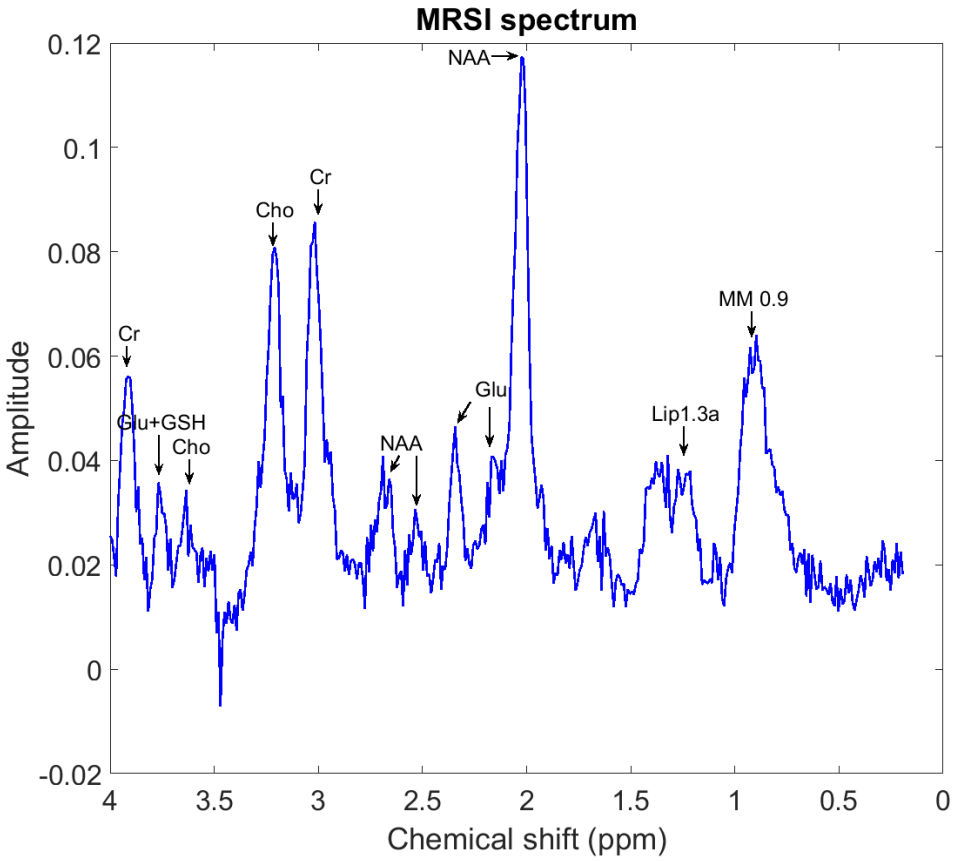

FIGURE A.1: ^{1}H NMR spectrum acquired at a field strength of 7T. Cr: creatine, Glu: glutamate, GSH: Glutathione, Cho: choline, NAA: N-acetylaspartate, Lip13a: lipid at 1.3ppm, MM0.9: macromolecule at 0.9ppm

overlap. Due to the use of a magnetic field of 7T or higher it becomes possible to distinguish these metabolites on the ^{1}H NMR spectrum [70].

Appendix B

LCModel characteristics

TABLE B.1: Control parameters used in LCModel. MM: macromolecule, FOPC: first order phase correction, PE: phosphorylethanolamine

Parameter	Value	Parameter	Value
sd of expectation value (degrees/ppm)	7	start analyzing at column	5
ppm start	4.0	end analyzing at column	40
ppm end	0.2	field strength (Hz per ppm)	3.0000e+02
nunfil	519	echo time (ms)	2.30
n metabolites to be excluded	8	hidden control parameter	0.3
n metabolites for individual plots	50	upper limit FOPC	20
n data slices	1	lower limit FOPC (degrees/ppm)	-20
n data rows	44	sample time (s)	3.333e-04
n data columns	44	expected value for FOPC	0
create table file	yes	exclude spectrum	'MM17'
create ps file	yes	exclude spectrum	'MM20'
create csv file	yes	exclude spectrum	'MM14'
create coraw file	yes	exclude spectrum	'MM12'
create coord file	yes	exclude spectrum	'MM09'
islice	1	exclude spectrum	'PE'
start analyzing at row	5	exclude spectrum	'Acetate'
end analyzing at column	40	exclude spectrum	'Alanine'

Appendix C

T1 values applied in T1 correction

TABLE C.1: T_1 values for WM and GM measured at a field strength of 7T, based on values determined by Xin et al. [40]. Cr: creatine, Cho: choline, mI: myo-inocitol, Gly: glycine PCr: phosphocreatine, NAA: N-acetylaspartate, NAAG: N-acetylaspartatylglutamate, GPC: glycerophosphocoline, Gln: glutamine, Glu: glutamate, Lip13ab: lipid at 1.3ppm, PC: phosphatidylcholine, Tau: taurine, GSH: glutathione

Metabolite	T_1 WM (s)	T_1 GM (s)
Cr	1.78	1.74
Cho	1.32	1.51
mI+Gly	1.19	1.28
Cr+PCr	1.78	1.74
NAA+NAAG	1.9	1.83
GPC+Cho	1.32	1.51
Glu+Gln	1.75	1.61
Gln	1.74	1.64
Glu	1.75	1.61
NAA	1.9	1.83
Lip13ab	0	0
NAAG	0.94	1.21
GPC	1.32	1.51
PC	1.32	1.51
PCr	1.78	1.74
Tau	2.09	2.15
Gly	1.19	1.28
mI	1.19	1.28
GSH	1.06	1.14
Macromolecules	0.42	0.43
Water	1.55	2